New skulls of the basal sauropodomorph *Plateosaurus trossingensis* from Frick, Switzerland: Is there more than one species?

JENS N. LALLENSACK, ELŻBIETA M. TESCHNER, BEN PABST, and P. MARTIN SANDER

The Triassic basal sauropodomorph *Plateosaurus trossingensis* is well-known from mass accumulations at the German localities of Trossingen and Halberstadt and the Swiss locality of Frick, and is significant especially regarding its taphonomy and proposed developmental plasticity. These implications, however, rely on the assumption that this material derives from a single species, which has been questioned. Here we describe new skull material from Frick including eight complete and six partial skulls, more than doubling the number of known skulls of *P. trossingensis*. This exceptional sample size allows for gaining a deeper understanding of variability that may occur in a single species. The new material includes the first known juvenile skulls of *Plateosaurus*, allowing for detecting ontogenetic changes. An attempt is made to distinguish between variability caused by taphonomic plastic deformation and intraspecific variability. Plastic deformation may shorten, but not widen bones. A number of characters commonly included in phylogenetic analyses of basal sauropodomorphs are shown to be variable within *P. trossingensis*, and possibly require re-evaluation. Although *P. trossingensis* skulls are highly variable, many of the variable characters include intermediate character states and therefore are continuous. No groupings based on skull features, locality, or stratigraphy are apparent. Consequently, the analyzed skull material from the bonebeds of Frick, Trossingen, and Halberstadt bears no evidence for the presence of more than one species.

Key words: Dinosauria, Sauropodomorpha, *Plateosaurus*, ontogeny, intraspecific variability, preservation, skull anatomy, Triassic, Switzerland.

Jens. N. Lallensack [info@dinospuren.de], Section Paleontology, Institute of Geoscience, University of Bonn, Nussallee 8, 53115 Bonn, Germany; School of Natural Sciences and Psychology, Liverpool John Moores University, James Parsons Building, Bryon Street, Liverpool L3 3AF, UK.
Elżbieta M. Teschner [eteschner@uni.opole.pl], Section Paleontology, Institute of Geoscience, University of Bonn, Nussallee 8, 53115 Bonn, Germany; Institute of Biology, University of Opole, Oleska 22, 45-052, Opole, Poland.
Ben Pabst [benpabst@bluewin.ch], Sauriermuseum Aathal, Zürichstrasse 69, 8607 Aathal-Seegräben, Switzerland.
P. Martin Sander [martin.sander@uni-bonn.de], Section Paleontology, Institute of Geoscience, University of Bonn, Nussallee 8, 53115 Bonn, Germany; Dinosaur Institute, Natural History Museum of Los Angeles County, 900 Exposition Boulevard, Los Angeles, CA 90007, USA.

Introduction

The basal sauropodomorph *Plateosaurus trossingensis* Fraas, 1913, from the Late Triassic of Central Europe is one of the best known Triassic dinosaur species (Galton and Upchurch 2004). The majority of the material, including dozens of partial to complete skeletons, stems from three localities: Trossingen and Halberstadt in Germany, and Frick in Switzerland (Sander 1992). These localities represent distinctive near-monospecific assemblages termed *Plateosaurus* bonebeds sensu Sander, 1992. Large-scale excavations in Trossingen and Halberstadt have been conducted during the first half of the 20th century but have halted since (but see Schoch and Seegis 2016). The fossil locality of Frick, the last bonebed to be discovered, is continuously being excavated since 1976, with the vast majority of *Plateosaurus* material still awaiting description.

The known *Plateosaurus* bonebeds are thought to have formed under similar taphonomic conditions. Their monospecific nature, the upright posture of the skeletons with the feet buried the deepest, the predominance of posterior

skeletal parts, the completeness of the remains, and the lack of juveniles has been interpreted as evidence for in situ miring in mud (Sander 1992). *P. trossingensis* may also allow for general insights into the evolution of endothermy—the lack of a strong correlation between ontogenetic age and body size indicates that this dinosaur, which was already endothermic, retained developmental plasticity, which is otherwise only known from ectothermic animals (Sander and Klein 2005; Klein and Sander 2007).

Galton (1984, 1985) assigned the sauropodomorph material from the bonebeds of Trossingen, Halberstadt, and Frick to a single species, *Plateosaurus engelhardti* (now *P. trossingensis*, see ICZN 2019), which was followed by many subsequent studies (e.g., Sander 1992; Moser 2003; Yates 2003). This classification, however, remained vague given the high degree of morphological variability and the stratigraphic uncertainties. Galton and Kermack (2010) referred the Halberstadt specimens to *Plateosaurus longiceps* and the Trossingen specimens to *P. trossingensis* based on differences in the pterygoid. The question regarding the number of species in these bonebeds is therefore far from being resolved, despite it being fundamental for the interpretation of these mass assemblages, and therefore requiring further testing. Most importantly, the presence of more than one species would question the developmental plasticity hypothesis of Sander and Klein (2005), because taxonomic diversity is the most parsimonious explanation to the observed lack of correlation between ontogenetic age and body size.

The purpose of the present paper is threefold: We aim to (i) describe the skull material from Frick for the first time in detail, (ii) assess the contribution of taphonomic deformation, ontogeny, and intraspecific variation to the morphological variability in *Plateosaurus* fossils, and (iii) test whether or not the bonebeds of Trossingen, Halberstadt, and Frick contain a single *Plateosaurus* species based on skulls. The material from Frick includes eight complete skulls, seven partial skulls, and a number of isolated or disarticulated skull bones, all of which are undescribed except for two partial skulls and several isolated elements described by Galton (1986). This material includes the first skulls of an early-stage as well as a late-stage juvenile, offering the first insights into ontogenetic changes of skull morphology in *Plateosaurus*. This new material from Frick more than doubles the number of known skulls of *Plateosaurus*. Together with two complete skulls from Halberstadt and four complete skulls from Trossingen, *P. trossingensis* is now known from a total of 14 complete skulls. The exceptional quantity of available skulls improves our understanding of preservational and intraspecific variability in basal sauropodomorphs, which has implications for taxonomy.

Institutional abbreviations.—AMNH FARB, American Museum of Natural History, Fossil Amphibian, Reptile, and Bird collection, New York, USA; GPIT, Institut und Museum für Geologie und Paläontologie der Universität Tübingen, Germany; MB.R., Museum für Naturkunde (collection of fossil Reptilia), Berlin, Germany; MSF, Sauriermuseum Frick, Frick, Switzerland; NAAG, Naturama Aargau, Aarau, Switzerland; SMA, Sauriermuseum Aathal, Aathal-Seegräben, Switzerland; SMNS, Staatliches Museum für Naturkunde, Stuttgart, Germany.

Material and methods

Skull material of *Plateosaurus* is known from the German localities of Trossingen (four complete and three partial skulls), Halberstadt (two complete and at least one partial skull), and Erlenberg (one partial skull) (Galton 1985), as well as from the Swiss locality of Frick (eight complete and six partial skulls, described herein). The three German localities can probably be referred to the Trossingen Formation (Schoch 2011; Galton 2012), while the Swiss locality is part of the Klettgau Formation (Jordan et al. 2016). In the locality of Trossingen, two distinct *Plateosaurus* bonebeds, an upper and a lower bonebed, are present at Obere Mühle, while Halberstadt and Frick exposed a single bonebed respectively (Sander 1992). All of the skull material from Trossingen mentioned herein stems from the lower bonebed of Trossingen (Galton 1985). Another skull from Trossingen (GPIT 18318a) stems from an older unit (middle Löwenstein Formation at Untere Mühle; Hungerbühler 1998) and has been referred to a separate species, *P. gracilis* (Yates 2003); this skull is not included in the present study.

The locality of Frick, which is primarily exposed in the active clay pit "Gruhalde" operated by the Tonwerke Keller AG, is the only *Plateosaurus* bonebed that is still being excavated (Fig. 1). Excavation started in 1976 after first bone fragments were discovered in 1962. The yield of the first excavations, led by Urs Oberli, has been described by Galton (1986) and included two partial skulls (SMA 5 and MSF 6), a braincase (MSF 2), and an isolated premaxilla and dentary (MSF 1). Since then, a great quantity of material was discovered, including a first complete skeleton with skull, discovered in 1985 by Beat and Thomas Imhof (MSF 23); a complete skull discovered in 1995 by the local museum Naturama Aargau; and six complete and five partial skulls discovered by an excavation team lead by one of us (BP) in annual excavation campaigns between 2004 and 2018. The majority of the material from Frick does belong to the repository of the Sauriermuseum Frick (MSF); the known and prepared skull material from Frick is listed in Table 1.

The material described herein includes the first known juvenile skulls of *Plateosaurus*. MSF 12.3 comprises a nearly complete and articulated skull and partial postcranium (femur length 44.7 cm); open neurocentral sutures indicate a late juvenile stage. MSF 15.8B is the disarticulated, partial skeleton of an early juvenile stage, as indicated by the small size (femur length: 24.3 cm) and the absence of suture closure (Nau et al. 2020). This specimen was found within a circular bone cluster (MSF 15.8) comprising ca. 2000 bones belonging to at least eight individuals. Referral of the post-
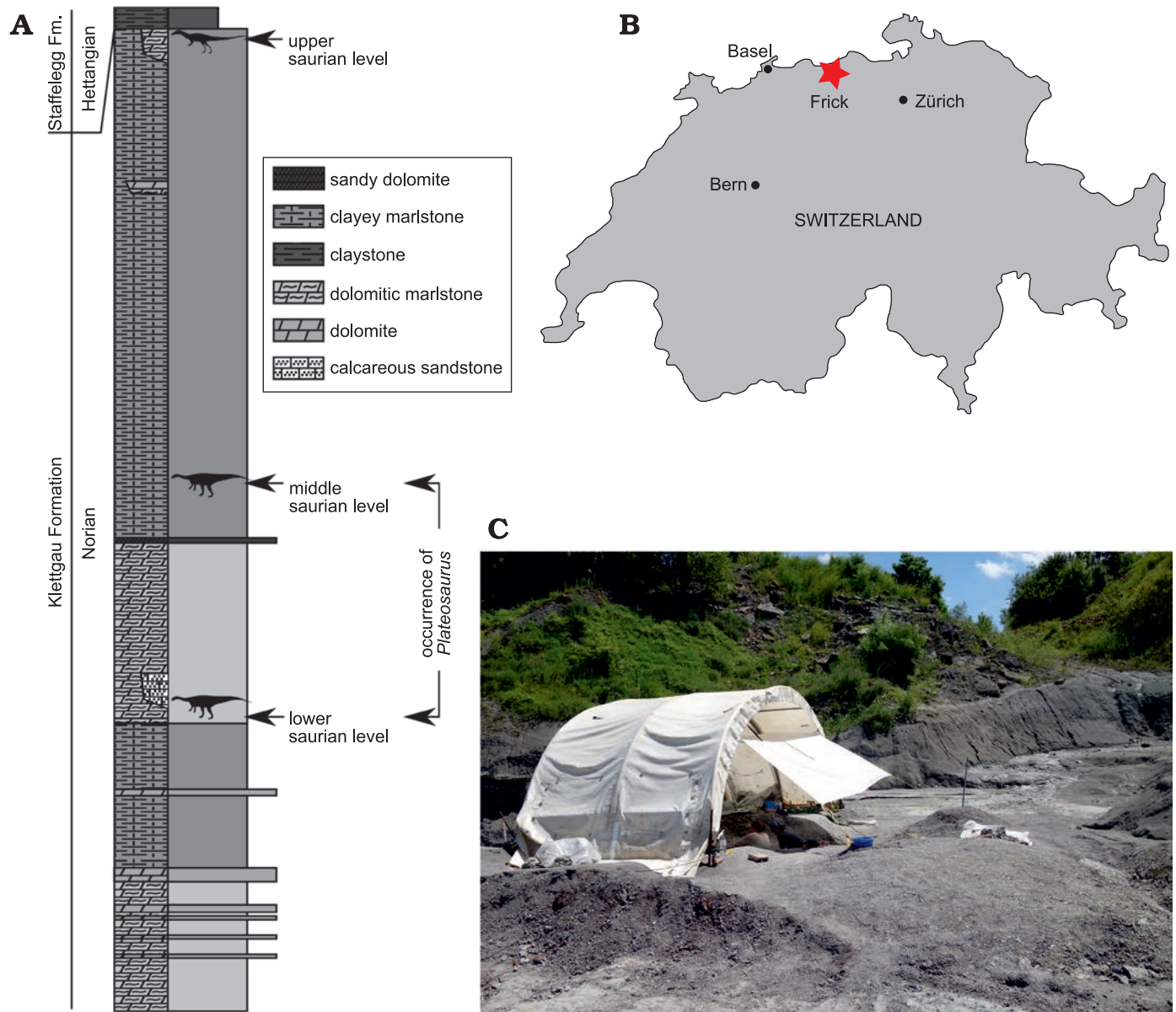
Fig. 1. **A**. Stratigraphic section of the Gruhalde Member of the Klettgau Formation as exposed in the Gruhalde Quarry in Frick, redrawn from Jordan et al. 2016 and Nau et al. 2020 (CC BY). The studied *Plateosaurus* material comes from the lower and middle bonebeds, which are separated by a dolomite marker horizon. **B**. Location of Frick (star) in Switzerland. **C**. Excavation of the find MSF 15.8 in the Gruhalde Quarry in July 2016.

cranial elements to a single individual was based on the consistently small size and the lack of elements that are represented twice (Nau et al. 2020). Several skull elements of MSF 15.8, including a premaxilla, a dentary, and a parietal, can be referred to the specimen based on their small size; the dentary measures approximately 50% of those of the adult *Plateosaurus* specimens studied herein. A prefrontal is comparatively larger, which is possibly due to a proportionally larger orbit (Reisz et al. 2005) if allometry is present in the skull; this element is preliminarily referred to MSF 15.8B as well. Two additional elements, a basisphenoid-parasphenoid (MSF 15.8.1043) and a squamosal (MSF 15.8.2030), have initially been listed as parts of MSF 15.8B (Nau et al. 2020), but are distinctly larger in size and therefore probably pertain to different individuals. The basisphenoid-parasphenoid is not

fused to its basioccipital, indicating a juvenile state—it could therefore possibly pertain to a second, larger juvenile individual of MSF 15.8 that is known from postcranial remains.

To assess the distribution of variable skull features in *P. trossingensis* as a whole, we also examined the skulls GPIT-PV-30784 (previously designated as GPIT/RE/9392, GPIT 1, or UT 1), SMNS 12949, SMNS 13200, SMNS 52967, SMNS 52968, and SMNS 12950 from Trossingen, as well as MB.R.1937 (previously HMN XXIV) and MB.R.4430.1 from Halberstadt. Our comparisons to AMNH FARB 6810 from Trossingen are based on the detailed descriptions of Galton (1984) and Prieto-Márquez and Norell (2011). Additional photographs of the examined skulls are provided in the SOM (Supplementary Online Material available at http://app.pan.pl/SOM/app66-Lallensack_etal_SOM.pdf).

Table 1. *Plateosaurus* skull material from the lower and middle "saurian levels" of Frick, Switzerland.

Specimen number	Material	Excavation	Repository	Reference
MSF 1	premaxilla and dentary, isolated	Urs Oberli 1976	Sauriermuseum Frick, Switzerland	Galton 1986
MSF 2	braincase	Urs Oberli 1976	Sauriermuseum Frick, Switzerland	Galton 1986
MSF 5	disarticulated skull	Urs Oberli 1976	Sauriermuseum Aathal, Aathal-Seegräben, Switzerland	Galton 1986
MSF 6	anterior part of skull and dentary	Urs Oberli 1976	Umwelt Arena Schweiz, Spreitenbach, Switzerland	Galton 1986
MSF 33	isolated dentary	Urs Oberli 1976	Sauriermuseum Frick, Switzerland	this study
MSF 23	complete skull	Beat and Thomas Imhof 1985	Sauriermuseum Frick, Switzerland	this study
NAAG_00011238	complete skull	Rainer F. Foelix 1995	Naturama Aargau, Aarau, Switzerland	this study
NAAG_00011239	partial skull, isolated elements	Rainer F. Foelix 1995	Naturama Aargau, Aarau, Switzerland	this study
MSF 07.M	braincase and lower jaws	Ben Pabst 2007	Museum of Natural Sciences, Brussels, Belgium	this study
MSF 08.M	partial skull with braincase	Ben Pabst 2008	University of Bonn, Germany	this study
MSF 08.H	isolated elements	Ben Pabst 2008	Sauriermuseum Frick, Switzerland	this study
SMA 09.1 (SMA 0255)	skull with braincase	Ben Pabst 2009	Sauriermuseum Aathal, Aathal-Seegräben, Switzerland	this study
MSF 09.2	partial skull	Ben Pabst 2009	Sauriermuseum Frick, Switzerland	this study
MSF 11.4	complete skull	Ben Pabst 2011	Sauriermuseum Frick, Switzerland	this study
MSF 12.3	complete skull	Ben Pabst 2012	Sauriermuseum Frick, Switzerland	this study
MSF 15.4	complete skull	Ben Pabst 2015	Sauriermuseum Frick, Switzerland	this study
MSF 15.8	juvenile skull (MSF 15.8B); isolated elements	Ben Pabst 2015–2016	Sauriermuseum Frick, Switzerland	this study
MSF 16.1	complete skull	Ben Pabst 2016	Sauriermuseum Frick, Switzerland	this study
MSF 17.4	complete skull	Ben Pabst 2017	Sauriermuseum Frick, Switzerland	this study

Photogrammetry.—Photogrammetric models of the cranial material from Frick, including all complete skulls, MSF 08.M, the braincase of MSF 07.M, and NAAG_00011239, were built using Agisoft Metashape Professional (www.agisoft.com), and are available in the SOM. Orthophotos as well as ambient occlusions, which enhance 3D morphology by shading points of the surface that are occluded by surrounding objects, were extracted from the 3D models using MeshLab (meshlab.net) and are shown in orthographic projection. Shading by low-angled virtual light was used in some cases to further enhance surface detail. In addition to the direct examination of the skulls, the digital 3D models displayed in orthographic projection were used for comparisons between specimens. Details on these visualization methods can be found in Lallensack et al. (2020). Photogrammetric models of the *Plateosaurus* skull material from Frick are available at https://doi.org/10.6084/m9.figshare.12890672.

Geology of the Gruhalde Quarry.—*Plateosaurus* remains in Frick stem from the middle part of the Gruhalde Member of the Klettgau Formation (Jordan et al. 2016), in a succession known as the "Obere Bunte Mergel" (Upper Variegated Marls). Although stratigraphical correlations are not possible at present, this succession is thought to be at least partly equivalent to *Plateosaurus*-bearing strata of Trossingen and Halberstadt, which are commonly considered late Norian in age (Sander 1992; Jordan et al. 2016). Etzold et al. (2010)

concluded that the lower bonebed of Trossingen is late Norian, while the upper bonebed is early Rhaetian in age.

The dinosaur-bearing section in Frick may be subdivided into three horizons. The *Plateosaurus* material analyzed herein stems from the lower two of these horizons, the lower and middle saurian levels, which are separated by a dolomite marker horizon (Fig. 1A). The time interval represented by these levels is unknown. The Gruhalde Member has been estimated to represent approximately 20 Myr, while the lower and middle saurian levels together account for 20% of the total thickness of the Gruhalde Member in the Gruhalde Quarry (Jordan et al. 2016); however, it cannot be necessarily assumed that the sedimentation rate was constant, and widespread pedogenesis may indicate sedimentation hiatuses.

The lower and middle saurian levels are mostly composed of grayish to variegated marl of high carbonate content that contain intraclasts and dolomite lenses. Layers are non-continuous, and the marl is cut by channel structures composed of silty marl to coarse-grained sandstone. While the majority of *Plateosaurus* fossils come from the marl, they can also be found in the sandstone. The marl has been interpreted as overbank deposits affected by pedogenesis within a terrestrial playa environment (Jordan et al. 2016).

The state of preservation of the *Plateosaurus* specimens found in Frick ranges from accumulations of a few bones to complete skeletons; isolated bones are relatively rare (Sander 1992). Specimen density is high, and the lateral distance between specimens is sometimes a few meters only. Exposures

of the horizons at the Frickberg at the other side of the Frick valley, almost 2 km away from the Gruhalde Quarry, contain equally abundant *Plateosaurus* remains and suggest an extent of the bonebed on the order of square kilometers.

Sauropodomorph remains, as well as the theropod *Notatesseraeraptor frickensis* Zahner and Brinkmann, 2019, were also found in the upper saurian level of the Gruhalde Quarry, immediately below the discordantly overlying marine sediments of the Early Jurassic (Zahner and Brinkmann 2019). The upper saurian level differs in lithology, and the bone material is black in color, not orange-gray as in the lower and middle levels, indicating different sedimentological conditions. As these sauropodomorph remains possibly represent a novel taxon (Zahner and Brinkmann 2019), they will be described elsewhere.

Results

Preservation.—*Plateosaurus* fossils from Frick are affected by plastic deformation (i.e., deformation without breakage) to a stronger degree than those from Trossingen and Halberstadt, complicating interpretation and causing loss of information (Fig. 2). The impact of such deformation on features of potential taxonomic relevance can be best studied by comparing mediolaterally compressed skulls with those that are compressed obliquely or dorsoventrally, and by analyzing left-right asymmetry in single skulls. Of the eight complete skulls, three are compressed mediolaterally, three obliquely, and two dorsoventrally. The deformation can be extreme, as seen in the case of the skull MSF 16.1, which is less than 10% as wide as long due to oblique lateral compression. In obliquely compressed skulls, the dorsal surface of the skull is often projected onto a single plane with the lateral surface, exposing the skull roof on one side of the skull but not on the other. This can be most clearly seen in MSF 16.1 (Fig. 3).

It is important to note, however, that plastic deformation only leads to shortening of fossils, but not to widening, because the sediment package containing the fossils is deformed as a whole (Fig. 2A; Walton 1936; Harris 1974; Rex and Chaloner 1983). This may be demonstrated based on the distal end of the right humerus of MSF 12.3, which is flattened anteroposteriorly to an extreme degree (Fig. 2B). Despite this extreme deformation, no widening is apparent in posterior view (parallel to the axis of deformation), and the ratio between the length and mediolateral width of this bone is almost equal to that of the relatively undeformed humerus of GPIT-PV-30785 (previously GPIT 2; 3.35 versus 3.37, respectively). Consequently, linear measurements tend to underestimate, but not overestimate, the original absolute dimensions, allowing to constrain the influence of deformation to some extent.

Below, we describe the effects of a simple compression assuming a single axis of deformation. These effects, which can be easily explored by transforming 3D models of skulls,
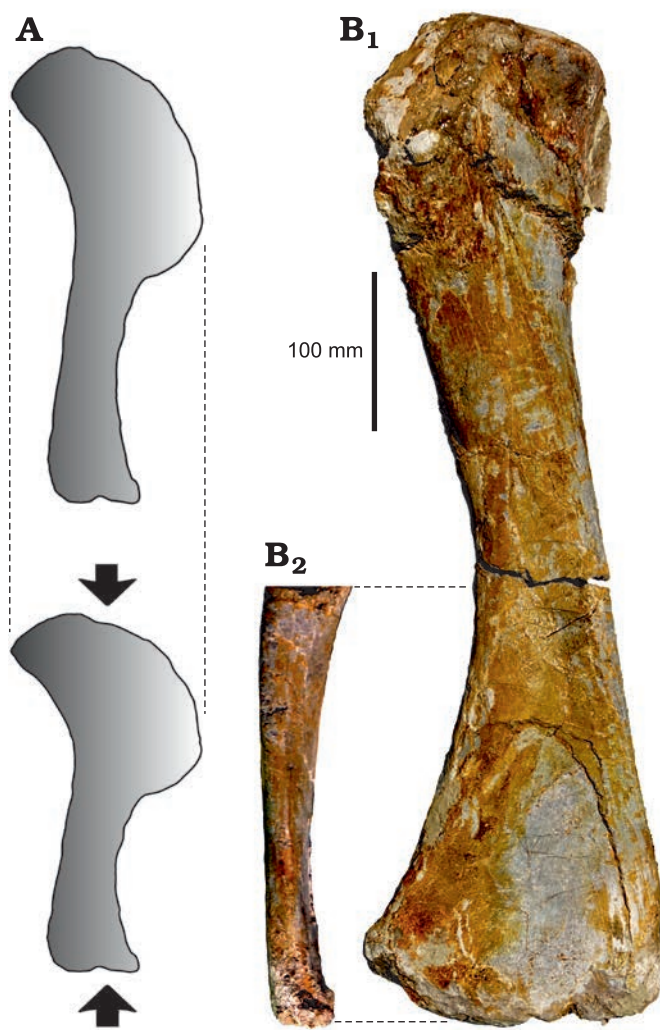

Fig. 2. Bone shortening due to plastic deformation. **A**. Compression may lead to substantial shortening along the axis of deformation. Note that no widening occurs. **B**. Right humerus of MSF 12.3 in posterior (B_1) and medial (B_2) views, showing extreme anteroposterior compression especially of the distal end. Despite this compression, the bone is not significantly widened in posterior view when compared with the relatively undeformed humerus of GPIT-PV-30785.

include changes in aspect ratios, angles, curvature, and relief. For example, mediolaterally compressed skulls will have a higher length-to-width ratio in dorsal and ventral views, and a lower height-to-width ratio in anterior and posterior views. Angles may become larger or smaller; for example, the angle between the paroccipital processes will be more acute in a mediolaterally compressed skull. The curvature and relief of a ridge is reduced when directed towards the axis of deformation, but exaggerated when directed parallel to it. These effects are determined by two factors: the magnitude of deformation and the orientation of the fossil relative to the axis of deformation. The latter factor determines how the original shape is projected onto the flattened fossil, and may be difficult to reconstruct, especially when the original orientation of the fossil within the sediment was not documented three-dimensionally. Slight variations in the orientation of the fossils will result in different projections, potentially
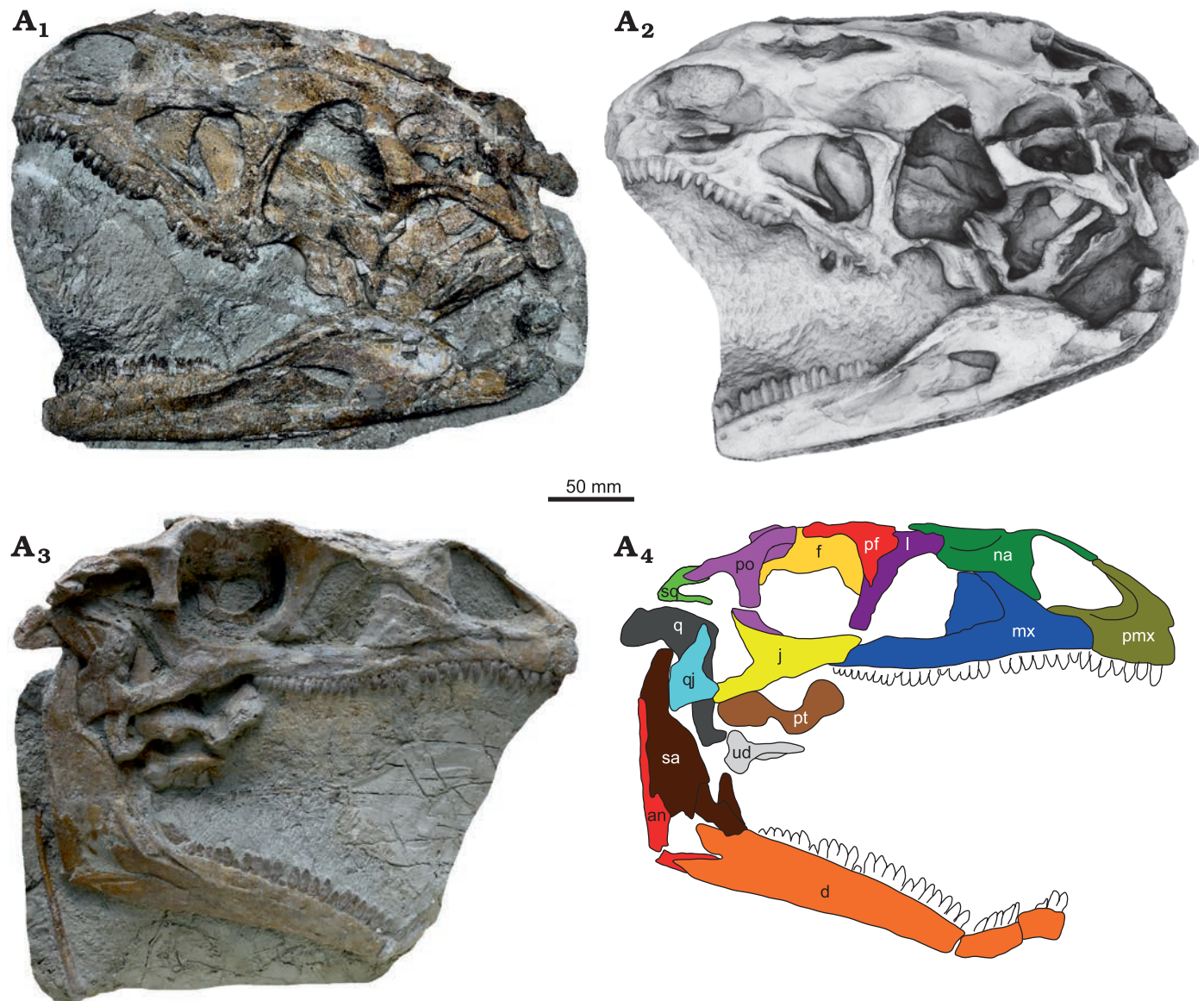
Fig. 3. Skull of *Plateosaurus trossingensis* (MSF 16.1) from the Triassic of Frick, Switzerland. Photograph of the left side (A$_1$); ambient occlusion of the 3D-model of the left side (A$_2$); photograph of the right side (A$_3$) and interpretative diagram (A$_4$). Abbreviations: an, angular; d, dentary; f, frontal; j, jugal; l, lacrimal; mx, maxilla; na, nasal; pf, prefrontal; pmx, premaxilla; po, postorbital; pt, pterygoid; q, quadrate; qj, quadratojugal; sa, surangular; sq, squamosal; ud, undefined.

leading to significant variation in apparent shape. If both the magnitude of deformation and the orientation of the fossil relative to the axis of deformation are known, the original shape may potentially be received through retrodeformation. This requires finding a combination of the two factors that meets assumptions such as symmetry between the left and right sides and known length-to-width ratios of elements. In practice, the magnitude of deformation is not relevant when the direction of view is parallel to the axis of deformation: a skull that was compressed dorsoventrally and does not show obvious skewing thus may preserve its approximate original shape in dorsal or ventral views, irrespective of the magnitude of deformation.

The model described above, however, can only partly explain the preservational variability in the examined skulls,

and therefore is an oversimplification. Although the fossil bearing layers are primarily composed of mudstone, they also contain sandstone and dolomite as well as intraclasts, and sediment composition may change at a small scale. Bones may also be appressed upon other bones, and the degree of ossification of the bone itself might further influence the magnitude of deformation (Fig. 2B; Hugi and Scheyer 2012). These factors may result in varying degrees of deformation, also within single elements. In addition to shortening along a single axis, the fossils may be affected by substantial shearing. This is best seen in MSF 11.4, where the left side of the skull is displaced anteriorly by almost 2 cm relative to the right side, resulting in an anteroposterior shortening of the left side of the skull by approximately 25% in relation to the right side (Fig. 4A$_5$, A$_6$).
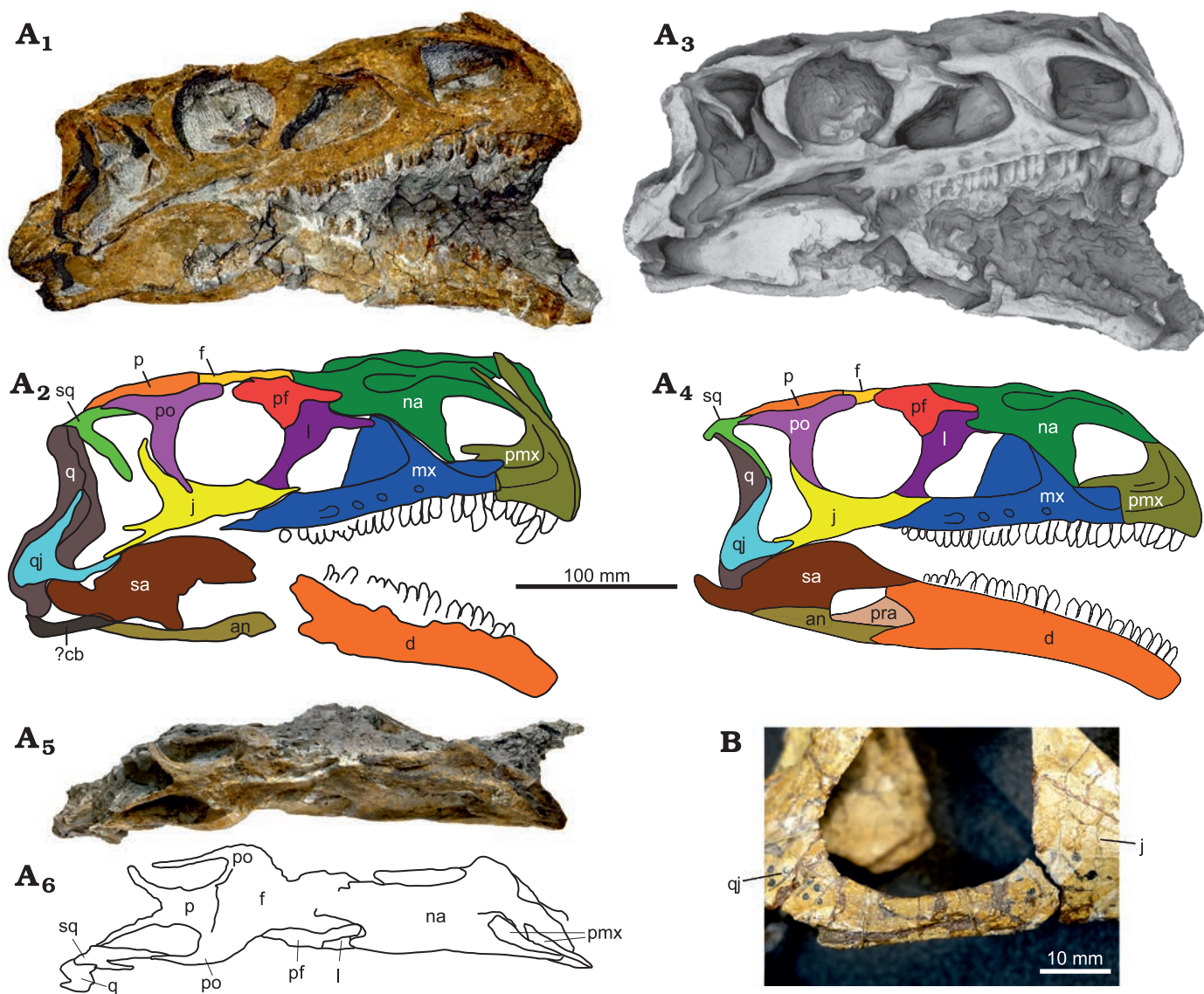
Fig. 4. **A**. Skull of *Plateosaurus trossingensis* (MSF 11.4) from the Triassic of Frick, Switzerland. Photograph of the right side (A$_1$) and interpretative diagram (A$_2$); ambient occlusion of the 3D-model of the right side (A$_3$) and interpretative diagram (A$_4$); photograph in dorsal view (A$_5$) and interpretative diagram (A$_6$). **B**. The jugal-quadratojugal articulation as seen in GPIT-PV-30784 from Trossingen. Abbreviations: an, angular; cb, ceratobranchial; d, dentary; f, frontal; j, jugal; l, lacrimal; mx, maxilla; na, nasal; p, parietal; pf, prefrontal; pmx, premaxilla; po, postorbital; pra, prearticular; q, quadrate; qj, quadratojugal; sa, surangular; sq, squamosal.

In addition to plastic deformation, mechanical crushing may also occur. This is most evident in MSF 16.1, where the right mandible is broken at the mandibular fenestra, with the dentary angled 110° relative to the posterior part of the mandible (Fig. 3). In MSF 15.4, the premaxilla is appressed onto an intraclast and fragmented (Fig. 5A$_1$, A$_2$). In MSF 23 (Fig. 6A), the articulated block composed of the postorbital, frontal, parietal, and squamosal was shifted anteriorly and ventrally, exposing the supratemporal fenestra in lateral view of the skull and reducing the orbit to a narrow slit while the antorbital fossa retains its original shape. A similar foreshortening of the orbit is seen on the right side of GPIT-PV-30784. Sander (1992) instead suggested that this foreshortening was the result of a characteristic disarticulation pattern.

Faults frequently occur in the fossil-bearing layers due to differential subsidence and may separate fossils into halves offset from each other, as seen, e.g., in the posterior part of the left side of the skull of MSF 16.1 (Fig. 3A$_1$, A$_2$). At a smaller scale, differential compression of separate parts of a bone can lead to the formation of shear zones whereby parts of the bone surface are depressed relative to other parts, as seen in the premaxilla of NAAG_00011238, for example (Fig. 7A$_1$, A$_2$).

Both articulated skulls and isolated skull elements are found at Frick, though the high proportion of articulated and complete skulls is remarkable even when accounting for the fact that some of the more fragmentary material still awaits preparation (Table 1). The Frick material encompasses eight nearly complete and articulated skulls as well as seven partial skulls of which three (MSF 09.2, MSF 08.M, MSF 6) are
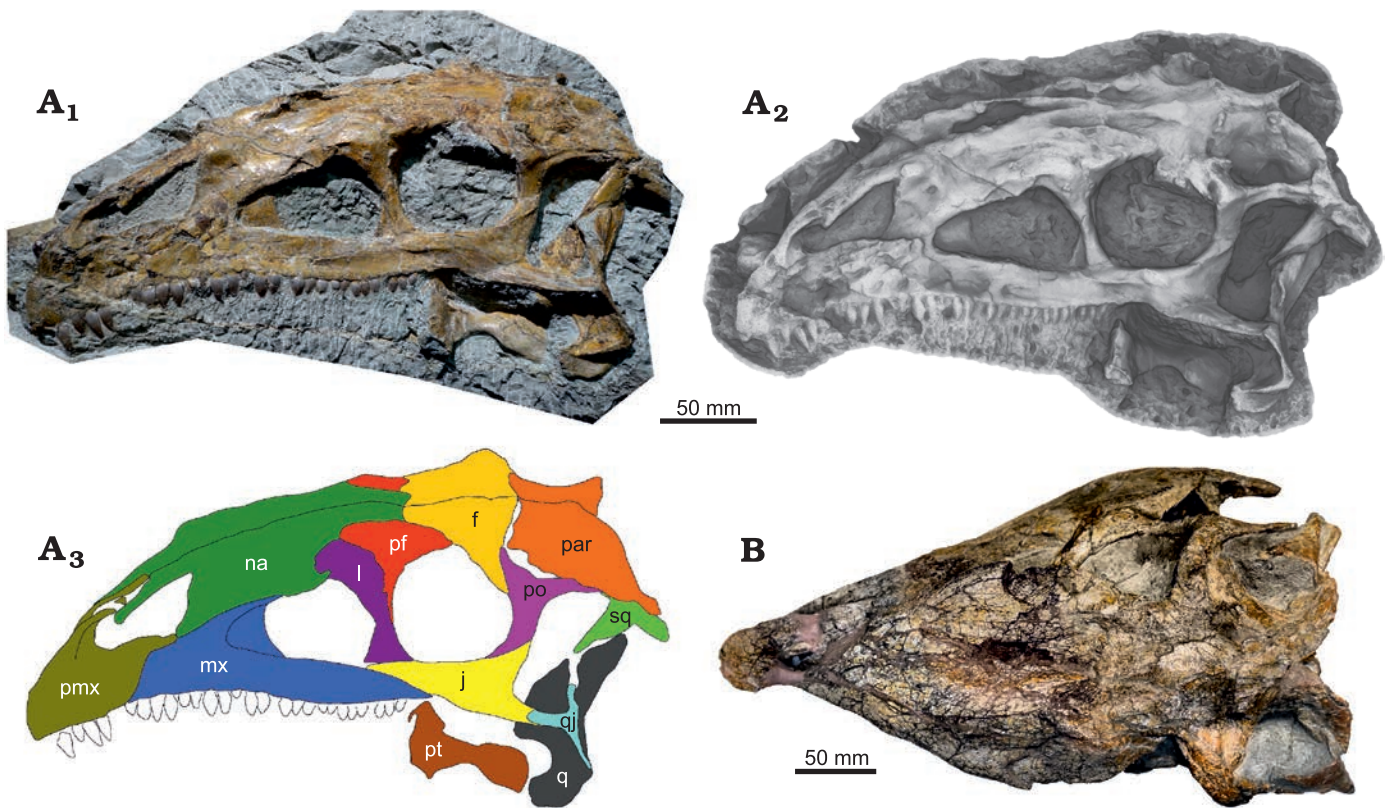
Fig. 5. **A**. Skull of *Plateosaurus trossingensis* (MSF 15.4) from the Triassic of Frick, Switzerland. Photograph in lateral view (A₁); **a**mbient occlusion of 3D-model (A₂); **i**nterpretative diagram (A₃). **B**. Photograph of SMNS 12949 in dorsal view. Abbreviations: f, frontal; j, jugal; l, lacrimal; mx, maxilla; na, nasal; par, paroccipital process; pf, prefrontal; pmx, premaxilla; po, postorbital; pt, pterygoid; q, quadrate; qj, quadratojugal; sq, squamosal.

articulated and two are disarticulated (MSF 5 and the juvenile MSF 15.8B). Of the articulated skulls, the degree of articulation varies. MSF 15.4, MSF 16.1, and NAAG_00011238 are best articulated, while in MSF 11.4 most elements are slightly shifted out of their anatomical position.

Sander (1992) proposed that disarticulation began at the nasofrontal suture, and that the posterior skull bones disarticulated more rapidly than those of the rostrum, with the nasal, premaxilla, and maxilla remaining as one unit. However, based on our much larger sample size, we now propose that the most frequent disarticulation in the complete skulls is that of the premaxilla (seen in MSF 17.4; MSF 23; MSF 12.3; MSF 11.4; SMNS 12949; GPIT-PV-30784); maxilla (seen in MSF 17.4; MSF 11.4; MSF 23); and jugal (seen in MSF 23; MSF 11.4; SMNS 12949; GPIT-PV-30784; missing in SMA 09.1, MSF 17.4 and on the left side of MSF 16.1).

Osteology.—*Size, proportions, and skull openings*: Skull size was quantified by measuring the anteroposterior length of the laterally exposed surface of the maxilla, because this measurement was available from the majority of skulls. In the eight articulated skulls from Frick, the lateral surface of the maxilla measures 16.1 cm on average. Only three of the skulls are notably larger or smaller: NAAG_00011238 is, at 20.3 cm (total skull length: 36.27 cm), the largest skull known from Frick and the largest of *Plateosaurus* from any locality. MSF 23 is, at 14.5 cm, probably the smallest adult

individual from Frick known from an articulated skull. Even smaller is MSF 12.3 at 12.5 cm. The early-stage juvenile MSF 15.8B (Nau et al. 2020) lacks the maxilla and is not included in this comparison; the length of the dentary of this specimen is 8.7 cm, measured from the distal tip to the anteriormost point of the gap between the posterodorsal and posteroventral process of the dentary. Excluding the juvenile skull MSF 12.3, the laterally exposed surface averages at 16.7 cm in length in the Frick skulls. Skulls from Trossingen and Halberstadt (SMNS 13200, SMNS 12950, SMNS 12949, GPIT-PV-30784, MB.R.1937, and AMNH FARB 6810) average at 16.6 cm. There is, therefore, no evidence for differences in body size between the three localities.

The skull of *Plateosaurus* is commonly reconstructed as mediolaterally narrow compared to other basal sauropodomorphs. However, the relative width of the skull is highly variable in known specimens, and mostly depends on the degree and direction of plastic deformation (Galton and Upchurch 2004). Published idealized skull reconstructions are likewise variable: the length-to-width ratio, measured from the posterior end of the parietal suture to the tip of the premaxillae and across the greatest width at the level of the postorbitals, varies between 2.0 in the reconstruction of Wilson and Sereno (1998: fig. 5A) and 2.27 in that of Galton and Upchurch (2004: fig. 12.2A). Because plastic deformation results in bone shortening but not widening, as was discussed above, skull width will be underestimated in the vast
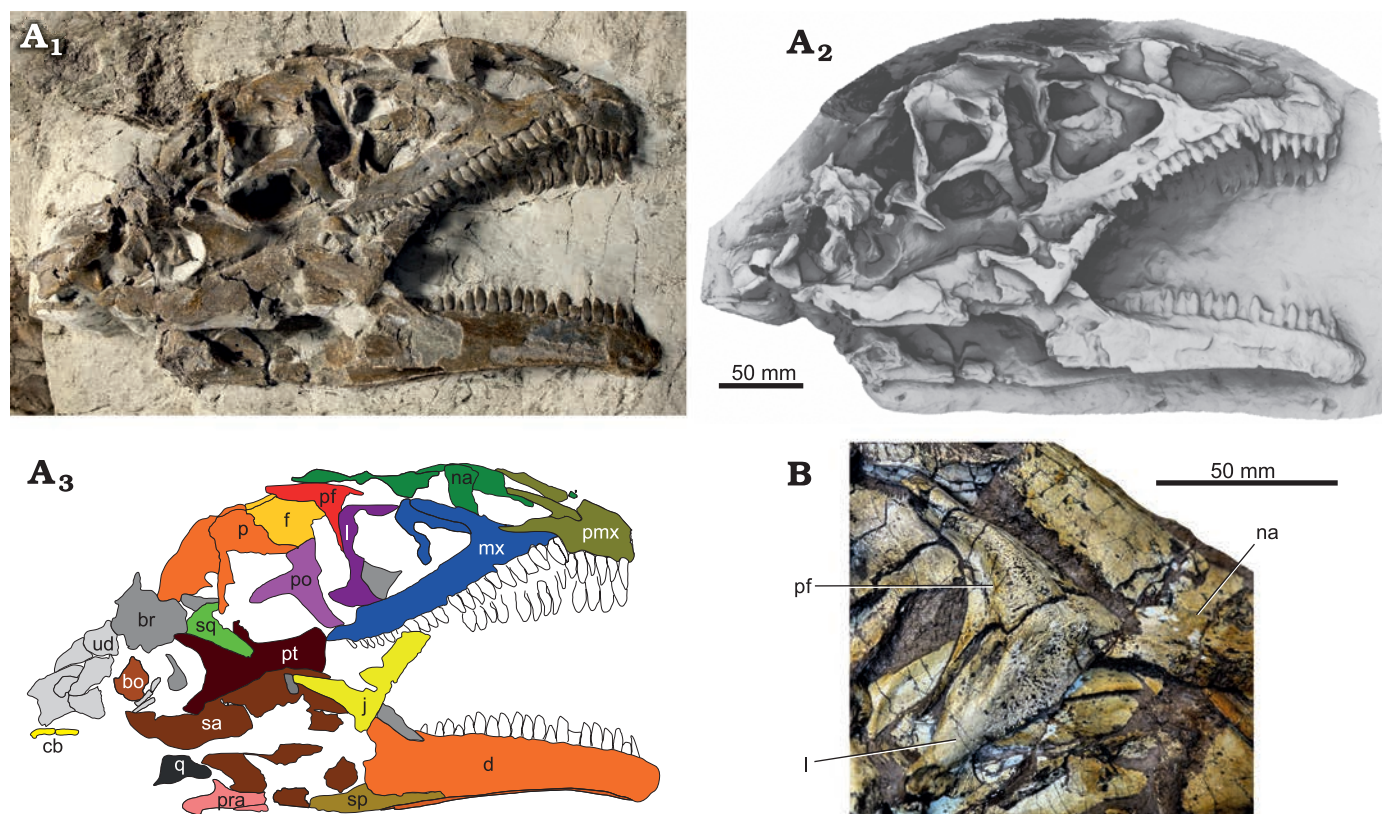
Fig. 6. **A**. Skull of *Plateosaurus trossingensis* (MSF 23) from the Triassic of Frick, Switzerland. Photograph in lateral view (A_1) (by Georg Oleschinski, University of Bonn, Germany); ambient occlusion of photogrammetric model (A_2); interpretative diagram (A_3). **B**. Detail of lacrimal and prefrontal of the right side of GPIT-PV-30784 from Trossingen. Abbreviations: bo, basioccipital; br, braincase; cb, ceratobranchial; d, dentary; f, frontal; j, jugal; l, lacrimal; mx, maxilla; na, nasal; p, parietal; pf, prefrontal; pmx, premaxilla; po, postorbital; pra, prearticular; pt, pterygoid; q, quadrate; sa, surangular; sp, splenial; sq, squamosal; ud, undefined.

majority of skulls, which are compressed mediolaterally. Of the articulated skulls from Trossingen and Halberstadt, only SMNS 12949 is primarily compressed dorsoventrally, suggesting that its length-to-width ratio of 2.2 is closer to the original ratio (Fig. 5B). This skull, however, is also skewed towards the left side, indicating a somewhat oblique main axis of deformation which may have caused mediolateral shortening as well. The only complete skull that lacks evident mediolateral shortening is the strongly dorsoventrally compressed skull of MSF 12.3 from Frick, which belongs to a late-stage juvenile and has a length-to-width ratio of 1.95, indicating a skull broader than in previous estimates for *Plateosaurus* (Fig. 8). We argue that these broader proportions may reflect the original proportions of *Plateosaurus* skulls in general, although we cannot fully dismiss the possibility that the proportions seen in MSF 12.3 were influenced by other possible factors such as skull elongation with ontogeny, intraspecific variability, or anteroposterior shortening due to plastic deformation.

The relative sizes of the external naris, antorbital fossa, and orbit are comparable in the skulls MSF 15.4, MSF 16-4, and NAAG_00011238, but are aberrant in MSF 11.4. In the latter, the maximum length of the antorbital fossa is 1.08 times that of the orbit (Fig. $4A_1$–A_4), while it is 1.2 to 1.3 in the other skulls. The external naris is small in MSF 11.4 at

0.66 times orbit length (Fig. $4A_1$–A_4), while it is between 0.94 and 1.02 in most other skulls. However, the external naris is similarly small in AMNH FARB 6010, and the antorbital fossa is similarly small in AMNH FARB 6010 and SMNS 12949, demonstrating that the same variability is present in the skulls from Trossingen. In NAAG_00011238, the infratemporal fenestra is markedly narrower anteroposteriorly compared to the orbit than in all other skulls (Fig. 7A).

The external naris is more or less triangular in shape, typically with a subvertical posterior margin, a subhorizontal ventral margin, and an anteroventrally inclined dorsal margin (e.g., Fig. $4A_4$). The anteroventral corner of the external naris can be broadly rounded, as in MSF 11.4 (Fig. $4A_1$–A_4) and SMNS 13200, or form a much more acute angle, as in MSF 16.1 (Fig. $3A_3$, A_4) and MB.R.1937. The latter condition is probably partly influenced by deformation. The ventral margin of the external naris is located dorsal to that of the antorbital fossa. The antorbital fossa is typically trapezoidal in shape, with a posterodorsally inclined anterior margin, a slightly posterodorsally inclined dorsal margin, and a anterodorsally inclined posterior margin (e.g., Fig. $4A_4$). The dorsal margin of the antorbital fossa is slightly (e.g., NAAG_00011238) or substantially (e.g., MB.R.1937) lower than the dorsal margin of the orbit; this variation
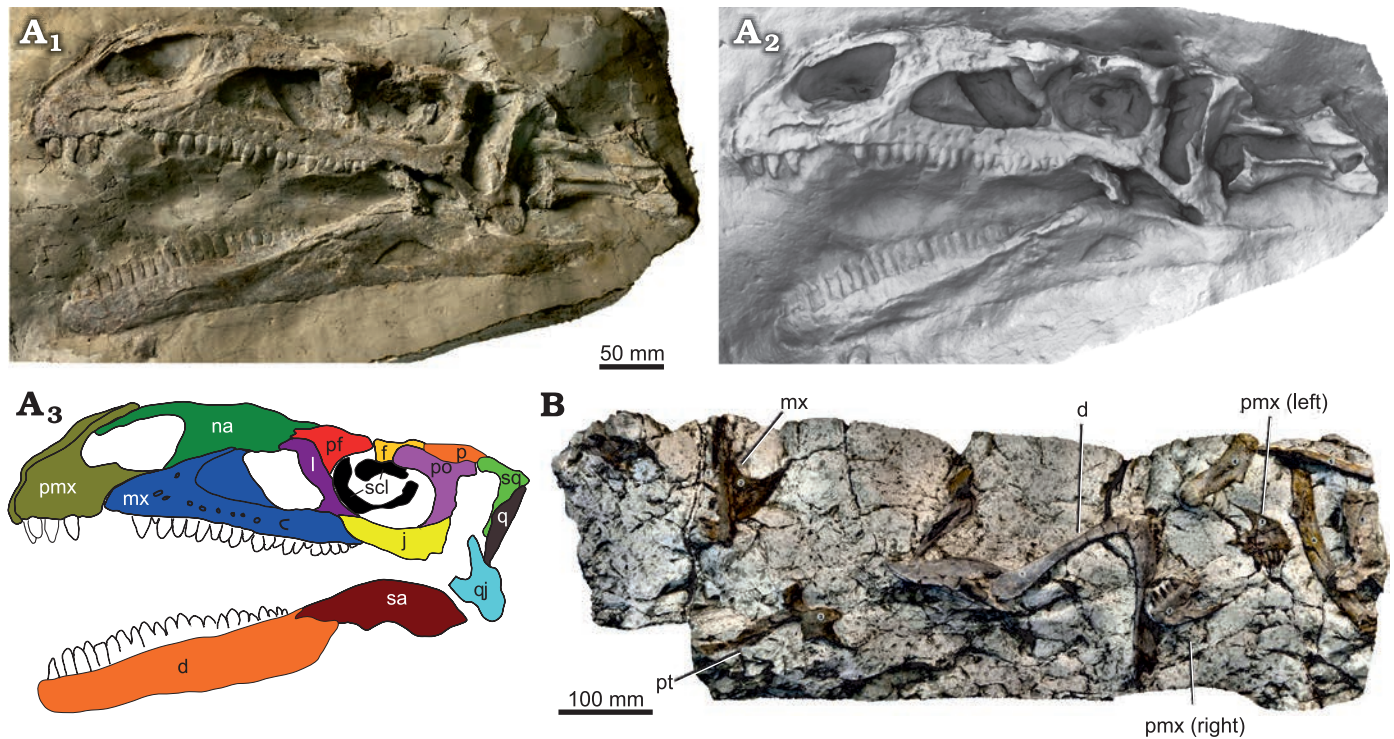
Fig. 7. **A**. Skull of *Plateosaurus trossingensis* (NAAG_00011238) from the Triassic of Frick, Switzerland. Photograph in lateral view (A₁) (by Georg Oleschinski, University of Bonn, Germany); ambient occlusion of photogrammetric model (A₂); interpretative diagram (A₃). **B**. Orthophoto of photogrammetric model of disarticulated skull material (NAAG_00011239). Abbreviations: d, dentary; f, frontal; fo, foramen magnum; j, jugal; mx, maxilla; na, nasal; p, parietal; pf, prefrontal; pmx, premaxilla; po, postorbital; pt, pterygoid; q, quadrate; qj, quadratojugal; sa, surangular; scl, sclerotic ring; sq, squamosal.

might be attributed to deformation. The orbit is subcircular and slightly longer than high (e.g., Fig. 4A₄); it is as long as high on the right side of MSF 16.1 (Fig. 3A₃, A₄). The infratemporal fenestra is dumbbell-shaped and anteroposteriorly constricted in the middle due to its convex posterior margin. The anterior margin of the infratemporal fenestra can be straight (e.g., MSF 15.4, Fig. 5A; MB.R.1937), or slightly convex (e.g., Fig. 4A₄) and contributing to the constriction. The dorsal half of the infratemporal fenestra is more narrow than the ventral half in MB.R.1937, while the opposite is the case in NAAG_00011238 (Fig. 7A); these differences are possibly due to plastic deformation. The extended posteroventral corner of the infratemporal fenestra (Pol and Powell 2007) that is strongly pronounced in SMNS 13200 appears to be the result of a deformation of the quadratojugal (see section "quadratojugal" below). The ventral margin of the infratemporal fenestra is substantially lower than that of the orbit in all skulls. The supratemporal fenestra is subtriangular in shape, with a posteromedially oriented anterior margin, a posterolaterally oriented posterior margin, and a anterolaterally oriented lateral margin (e.g., MSF 12.3, Fig. 8A₁, A₂; SMNS 13200; SMNS 12949; MB.R.1937).

Premaxilla: The premaxilla consists of a main body as well as a dorsal and a posterior process, which delimit the external naris in its anterior, anterodorsal, and ventral extents. There are five premaxillary tooth positions in SMA 09.1, in NAAG_00011238, the two premaxillae of NAAG_00011239,

MSF 12.3, MSF 1, MSF 15.8B, and probably MSF 15.4, while MSF 23, MSF 16.1, and MSF 11.4 show six premaxillary tooth positions. The main body of the premaxilla is longer than high in all skulls. In juvenile to subadult individuals of *Mussaurus* and *Massospondylus*, the premaxilla is shorter relative to its height than in adults (Pol and Powell 2007). In the late-stage juvenile MSF 12.3, the left premaxilla is indeed shorter than in any other of the examined skulls (Fig. 8A₁, A₂), but this is at least partly the result of shortening due to plastic deformation. The premaxilla is elongated in the early-stage juvenile MSF 15.8B (Fig. 9A).

The ventral margin of the premaxilla is straight or slightly concave in most specimens from Frick (MSF 12.3, MSF 15.4, NAAG_00011238, SMA 09.1, MSF 16.1, MSF 1) and in the examined skulls from Trossingen and Halberstadt, but is strongly curved and sloping ventrally in MSF 11.4 (Fig. 4A₁–A₄) and the juvenile specimen MSF 15.8B (Fig. 9A), although the latter lacks the distal tip of the premaxilla. A ventrally sloping premaxilla was found to be present in *Massospondylus* (Chapelle and Choiniere 2018). The anterior margin of the main body of the premaxilla is typically rounded, with the anteriormost point somewhat elevated above the level of the alveolar margin (e.g., MSF 11.4, Fig. 4A₁–A₄), but can be relatively straight (e.g., SMNS 52968), although not reaching the very straight condition seen in *Massospondylus* (Chapelle and Choiniere 2018; McPhee et al. 2019). *Plateosaurus* has been coded as having
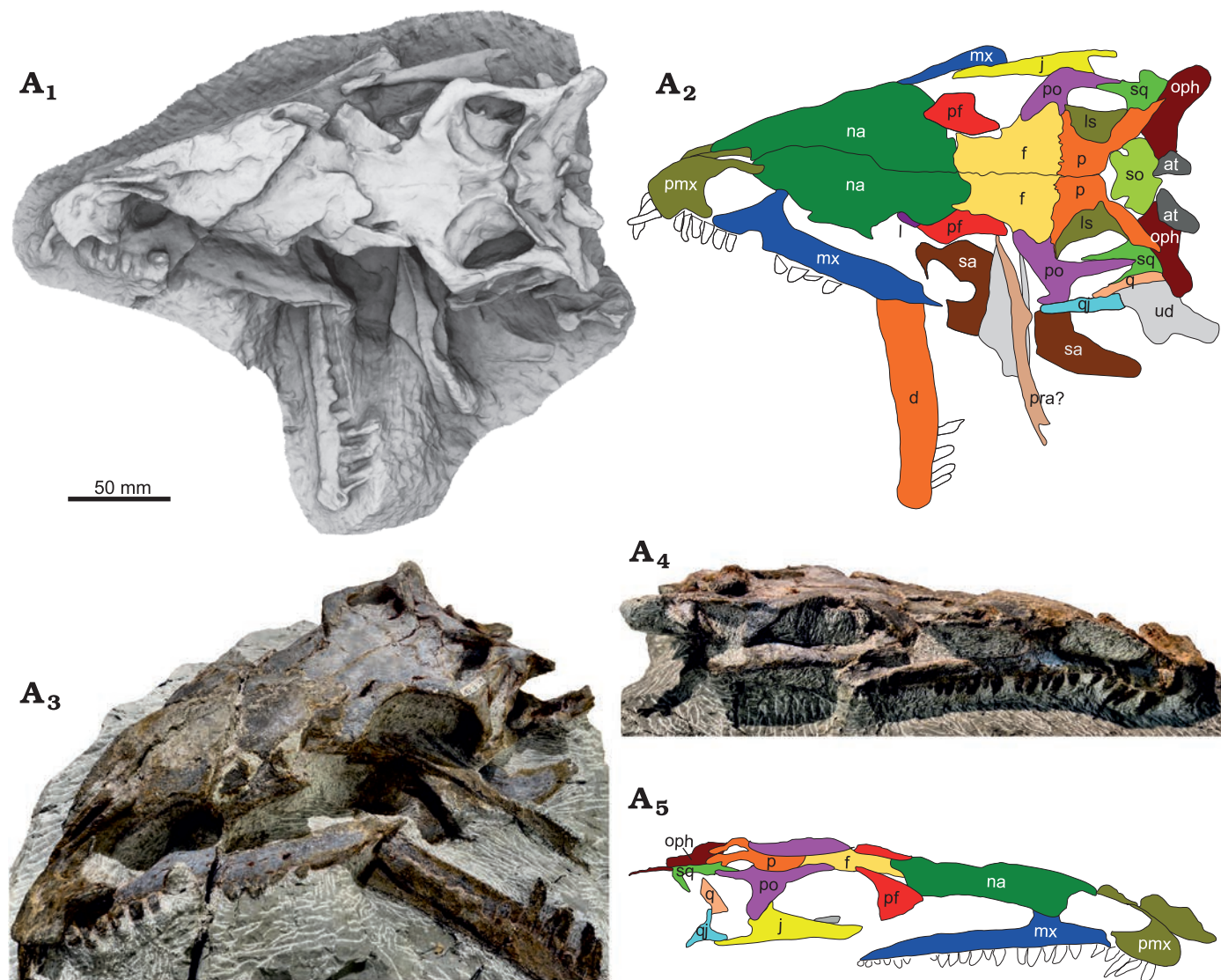
Fig. 8. **A**. Skull of the late-stage juvenile *Plateosaurus trossingensis* (MSF 12.3) from the Triassic of Frick, Switzerland. Ambient occlusion of photogrammetric model in dorsal view (A_1) and interpretative diagram (A_2); photograph of the skull in oblique view (A_3); photograph of the right lateral view (A_4) and interpretative diagram (A_5). Abbreviations: at, atlas; d, dentary; f, frontal; j, jugal; l, lacrimal; ls, laterosphenoid; mx, maxilla; na, nasal; oph, opisthotic; p, parietal; pf, prefrontal; pmx, premaxilla; po, postorbital; pra, prearticular; q, quadrate; qj, quadratojugal; sa, surangular; so, supraoccipital; sq, squamosal; ud, undefined.

a convex anterodorsal margin of the premaxilla without an inflection at the base of the dorsal process (Upchurch 1995; Yates 2007). However, such an inflection is pronounced in NAAG_00011238 and the disarticulated premaxilla of NAAG_00011239 (Fig. 7), and is also seen in MB.R.1937 from Halberstadt and SMNS 52968 from Trossingen. It is only weakly pronounced in MSF 11.4 and the juvenile MSF 15.8B, and absent in SMNS 13200 and AMNH FARB 6810 (Prieto-Márquez and Norell 2011).

Dorsally, the main body of the premaxilla borders both the external naris and the narial fossa. The anterior extent of the external naris is at approximately 20–25% of the length of the main body of the premaxilla, as seen in MSF 11.4, NAAG_00011238, MSF 16.1, and MSF 15.4. The anterior extent is slightly larger in the juvenile specimen MSF 15.8B (Fig. 9A). *Plateosaurus* skulls from Trossingen show

a greater variability: in ANMH FARB 6810, the anterior extent of the external naris is almost level with the posterior margin of the main body of the premaxilla (Prieto-Márquez and Norell 2011), while the external naris extends as far as 30% on the right side of SMNS 13200. The narial fossa is continuous with the dorsal surface of the posterior process and the ventral surface of the dorsal process, and delimited anteriorly, dorsally and ventrally by a rim, as best seen in MSF 11.4 (Fig. $4A_1$, A_3), but also in MSF 16.1 (Fig. 3), MSF 1, SMNS 52968, SMNS 13200, and MB.R.1936. In MSF 1, the rim is broad and elevated above the lateral surface of the main body of the premaxilla; this could, however, be the result of differential deformation of the central part of the premaxilla. The extent of the narial fossa is variable. It is smallest in SMA 09.1, where the distance between the anterior extent of the external naris and that of the narial fossa
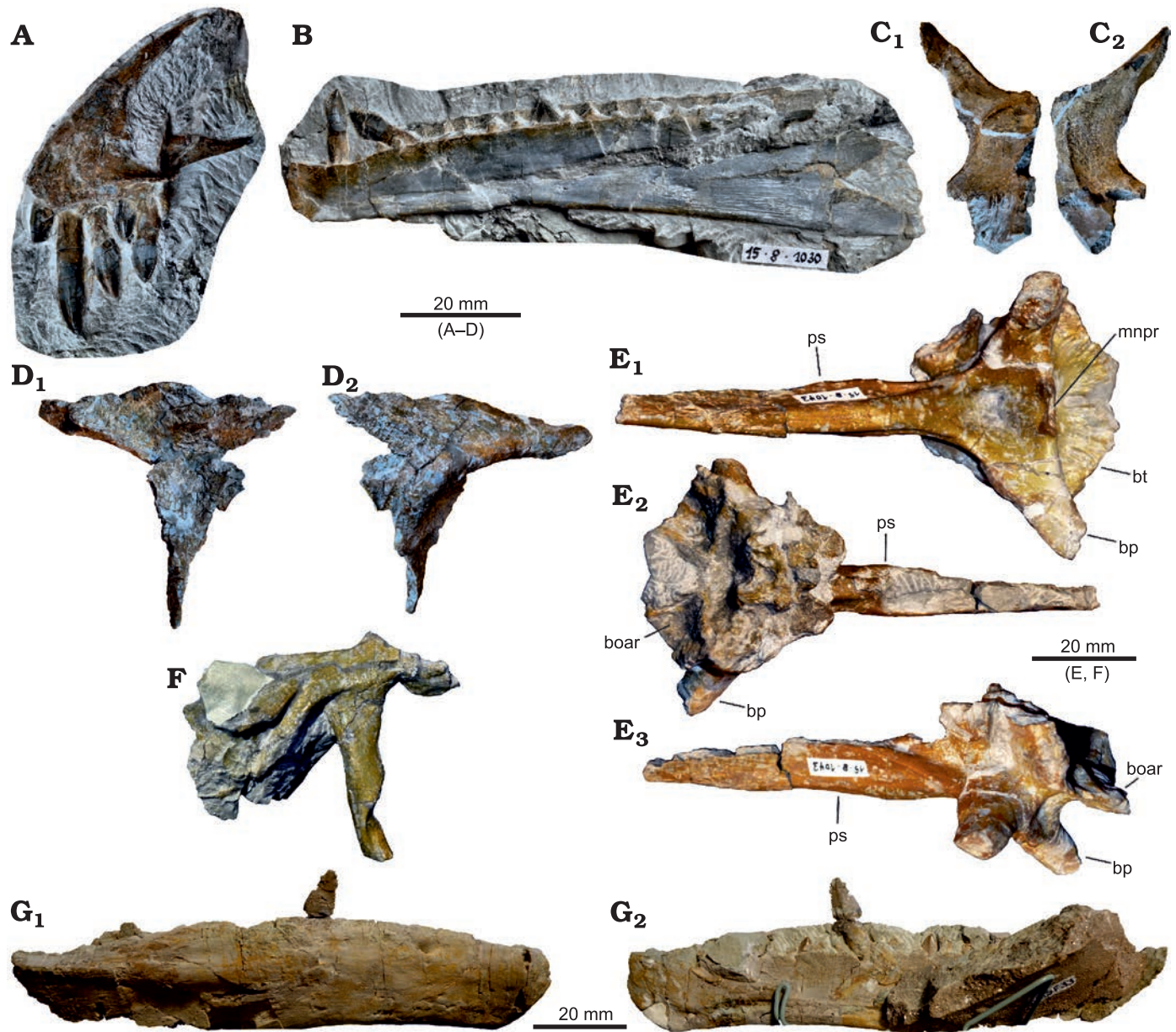
Fig. 9. *Plateosaurus trossingensis* material from the Triassic of Frick, Switzerland. **A–D**. Disarticulated skull of the early-stage juvenile (MSF 15.8B). **A**. MSF 15.8.935, premaxilla in medial view. **B**. MSF 15.8.1030, dentary in medial view. **C**. MSF 15.8.2029, left parietal in ventral (C_1) and dorsal (C_2) views. **D**. Left prefrontal (MSF 15.8.2028), in medial (D_1) and lateral (D_2) views. **E, F**. Isolated skull fragments pertaining to different individuals. **E**. Basisphenoid and parasphenoid (MSF 15.8.1043), in ventral (E_1), dorsal (E_2), and posterolateral (E_3) views (photographs by Ursina Bachmann). **F**. Left squamosal (MSF 15.8.2030) in lateral view (photograph by Ursina Bachmann). **G**. Isolated dentary (MSF 33), in lateral (G_1) and medial (G_2) views. Abbreviations: boar, articular surface for basioccipital; bp, basipterygoid process; bt, basipterygoid tubera; mnpr, median process; ps, parasphenoid.

is ca. 20% of the length of the main body of the premaxilla (Fig. 10A). It is largest in MSF 11.4, where this distance is 40% of the main body of the premaxilla, or nearly half of the premaxillary tooth row; in this specimen, the narial fossa is especially deep (Fig. 4A_1, A_3). The extent of the narial fossa is similarly variable in the skulls from Trossingen and Halberstadt, being small in SMNS 52968 (22%) and large in SMNS 13200 and MB.R.1936 (33% and 35%, respectively). As best seen in MSF 11.4, the narial fossa itself is located within a depression ventral and anterior to the narial fossa that is delimited by a sickle-shaped margin (Fig. 4A_1–A_4).

Ventral to this depression, the elevated portion of the lateral surface of the premaxilla is confluent with the very low lateral surface of the maxilla, as seen in MSF 11.4 (Fig. 4A_1–A_4). The depression is also seen in SMNS 52968 from Trossingen and MB.R.1936 from Halberstadt. The right premaxilla of NAAG_00011239 has a large, elongated foramen at the anterior edge of the base of the dorsal process just outside the narial fossa.

The dorsal process is dorsoventrally high at the base, while its distal portion becomes dorsoventrally thin and gradually broadens transversely in all skulls where this fea-
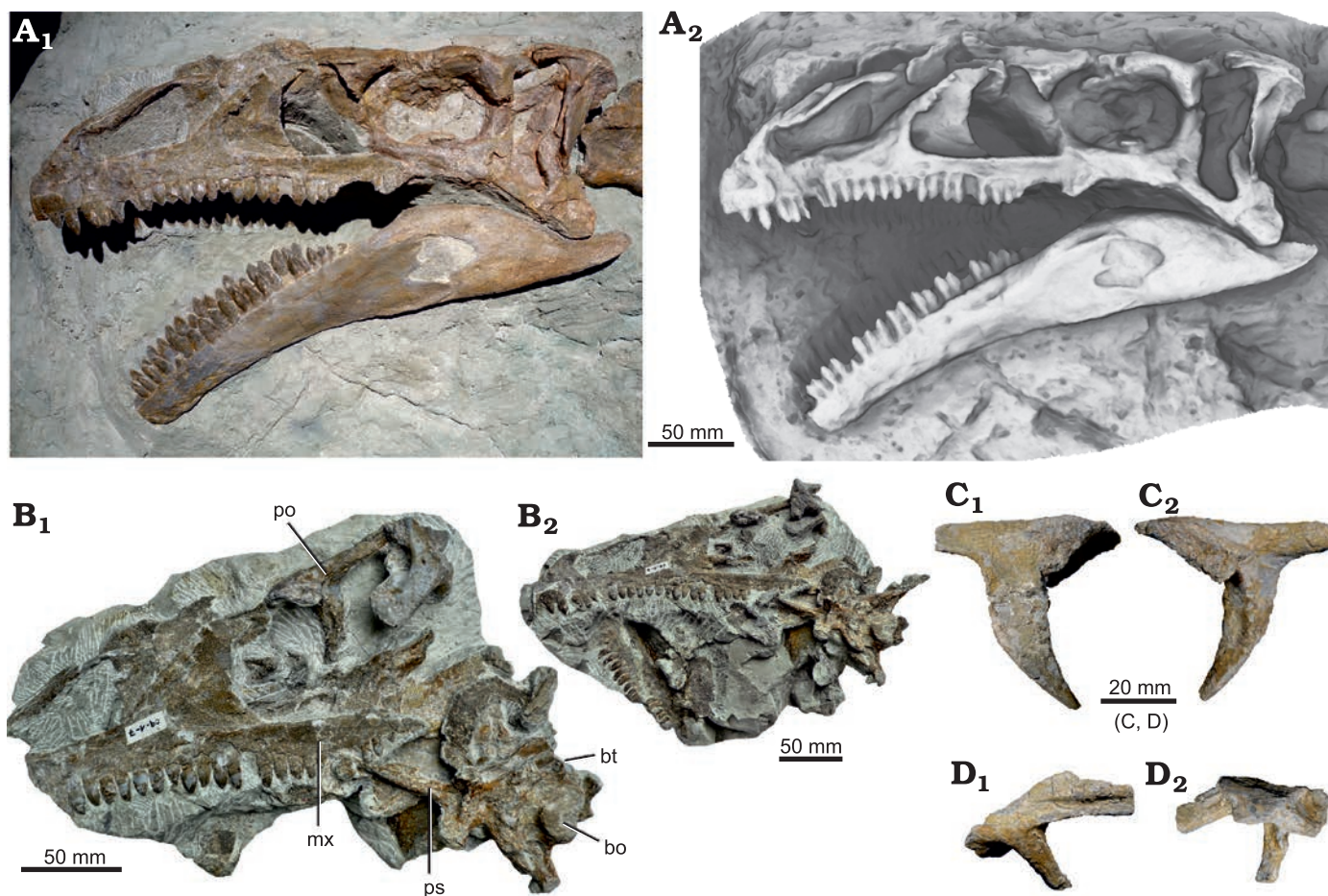
Fig. 10. **A**. Skull of *Plateosaurus trossingensis* (SMA 09.1) from the Triassic of Frick, Switzerland. The skull on exhibit at the Sauriermuseum Aathal (SMA) (A$_1$); note that parts posterior to the nasal, maxilla, and dentary are casted from NAAG_00011238; ambient occlusion of the museum exhibit (A$_2$). **B**. Photograph of the skull during preparation, showing additional elements in place (B$_1$); photograph of the skull at an early stage of preparation (B$_2$). **C**. Right postorbital in lateral (C$_1$) and medial (C$_2$) views. **D**. Right squamosal in lateral (D$_1$) and medial (D$_2$) views. Abbreviations: bo, basioccipital; bt, basipterygoid tubera; mx, maxilla; po, postorbital; ps, parasphenoid.

ture is observable. It extends distally between 80 and 90% of the dorsal margin of the external naris, as seen in MSF 15.4 (Fig. 5A) and SMA 09.1 (Fig. 10A). The dorsal process is most anteriorly sloping in the juvenile specimen MSF 15.8B, where its proximal half is inclined at an angle of 35° (Fig. 9A); the process is less steeply sloping in other skulls. The dorsal process is slightly curved along its length. Apaldetti et al. (2014) stated that the proximal part of the process is straight in massospondylids; this, however, also applies to some skulls of *Plateosaurus*, most obviously in MB.R.1937. The posterior process of the premaxilla extends to the posteroventral corner of the external naris, where it contacts the ventral process of the nasal (e.g, Fig. 5).

Maxilla: The maxilla consists of an elongated main body and a dorsal process that forms the anterior margin of the antorbital fenestra and fossa. The maxilla contains 23 tooth positions in NAAG_00011238; 28 on the left and a minimum of 25 on the right side in MSF 16.1; 24 in MSF 15.4; 22 in MSF 11.4; 24 in MSF 23; ca. 24 in the right maxilla and at least 22 in the left maxilla of SMA 09.1; and a minimum of 22 in the sub-adult MSF 12.3. Galton and Upchurch (2004) argued that the maxillary tooth row extends posteriorly to a level below the middle of the orbit in *Plateosaurus*. This feature was also found to be present in *Coloradisaurus*, *Lufengosaurus*, and *Mussaurus*, and was argued to distinguish these forms from other basal sauropodomorphs such as *Massospondylus* (Galton and Upchurch 2004). However, in all examined skulls, the maxillary tooth row does only slightly overlap the orbit. Only the left side of the Trossingen skull SMNS 13200 shows the tooth row extending until the middle of the orbit; this is, however, probably the result of an anterior displacement of the prefrontal and surrounding bones due to plastic deformation. In the right side of this skull, the tooth row only extends for 23% of the diameter of the orbit, comparable to other *Plateosaurus* skulls.

In all specimens, the ventral margin of the maxilla is slightly concave in its anterior half and convex in its posterior half. Anterior to the dorsal process, the dorsal part of the main body is recessed and separated from the lateral surface of the maxilla by a curved margin. Posteriorly, this border is continuous with the anterior edge of the dorsal process, and
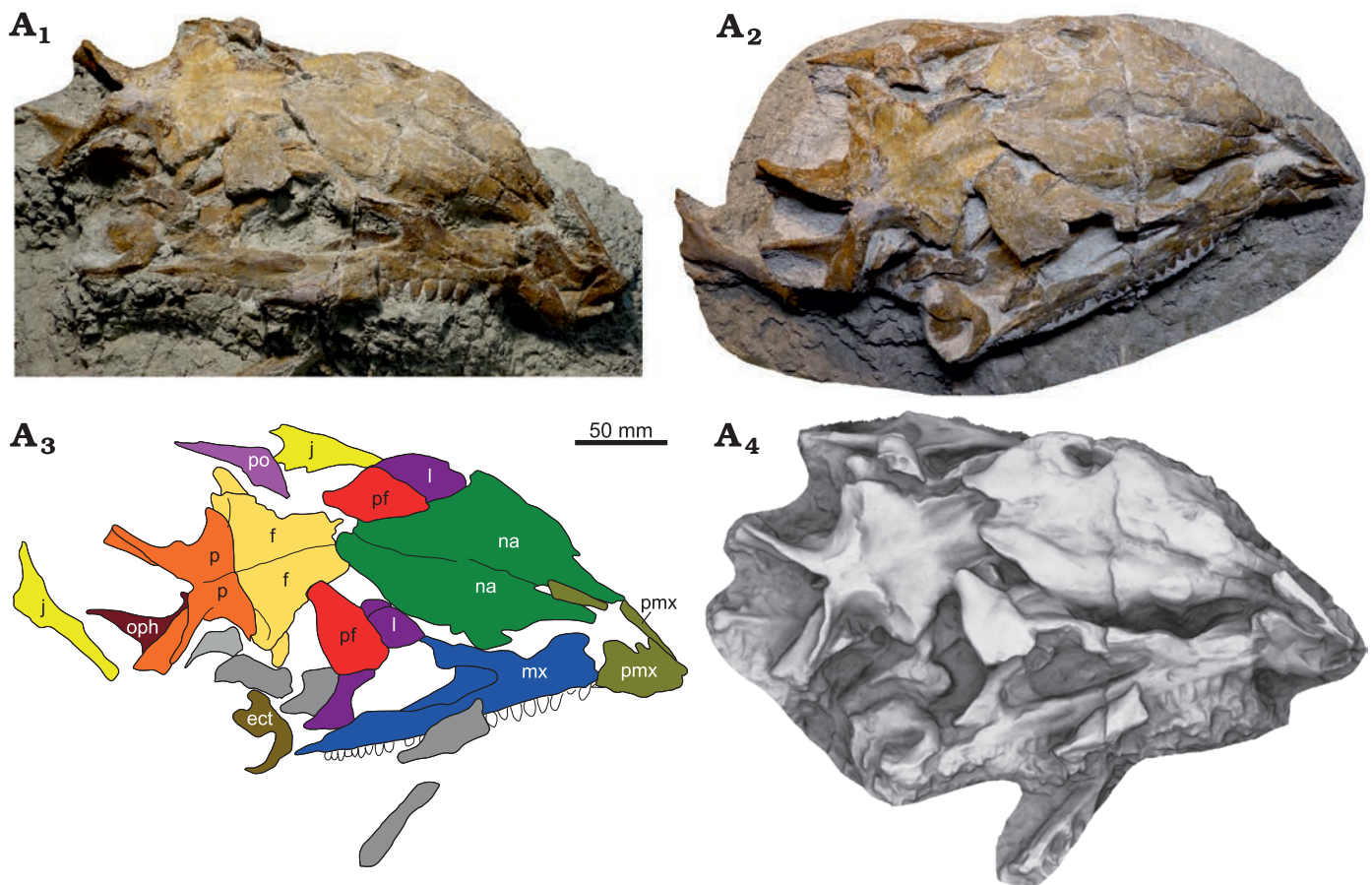
Fig. 11. Skull of *Plateosaurus trossingensis* (MSF 17.4) from the Triassic of Frick, Switzerland. Photograph of the skull in dorsolateral view at an early stage of preparation (A₁); photograph of the skull in oblique dorsolateral view at the final stage of preparation (A₂), note the additionally exposed jugal; interpretational diagram (A₃); ambient occlusion of photogrammetric model of the preparation state shown in A₁ (A₄). Abbreviations: ect, ectopterygoid; f, frontal; j, jugal; l, lacrimal; mx, maxilla; na, nasal; oph, opisthotic; p, parietal; pf, prefrontal; pmx, premaxilla; po, postorbital; ud, undefined.

anteriorly it continues up to the suture with the premaxilla, strongly reducing the dorsoventral height of the lateral surface of the maxilla in its anteriormost portion. This border is very pronounced in MSF 11.4 (Fig. 4A₁–A₄), but only weakly developed in NAAG_00011238 and seemingly absent in SMA 09.1 (Fig. 10A), which is probably at least partly due to mediolateral plastic deformation. The part of the main body of the maxilla posterior to the dorsal process is very variable in dorsoventral height in the different specimens. It is especially high in MSF 23, MSF 12.3, and MSF 09.2, where the level of the ventral margin of the antorbital fenestra is only slightly lower than that of the ventral margin of the external naris (Figs. 5A, 7A₃, B, 10). In contrast, it is shallow in NAAG_00011238 and especially in SMA 09.1, with the ventral margin of the antorbital fenestra located well below the ventral margin of the external naris (Figs. 7A, 10A). Similar variation is present in the examined skulls from Trossingen: in GPIT-PV-30784, the dorsoventral height of the maxilla anterior to the dorsal process is equal to the height posterior to the latter, while in SMNS 52968 the posterior part is only about 65% of the height of the anterior part.

Typically, the dorsal margin of the main body of the maxilla descends just posterior to the anterior rim of the dorsal process, but rises again towards the posteroventral corner of the antorbital fenestra, forming an apex near the anteriormost extent of the jugal. This morphology, which creates a concave floor of the antorbital fossa, is among the Frick skulls best seen in MSF 11.4 (Fig. 4A₁–A₄), but also in MSF 17.4 (Fig. 11) and, less pronounced, in MSF 12.3 (Fig. 8) and NAAG_00011238 (Fig. 7A). Other skulls, however, show an aberrant morphology: In MSF 09.2, the main body of the maxilla becomes dorsoventrally high already at mid-length of the maxilla, and the floor of the antorbital fossa is slightly convex rather than concave (Fig. 12). In MSF 15.4, the lateral surface of the maxilla ventral to the antorbital fossa is deepest just posterior to the anterior rim of the dorsal process and decreases gradually to the posteroventral corner of the antorbital fenestra (Fig. 5A). Again, similar variation is present in the examined skulls from the German localities, with SMNS 13200, SMNS 52967, AMNH FARB 6810, and MB.R.1937 showing a concave floor of the antorbital fossa while the floor is straight or slightly convex in SMNS 12950.

A number of neurovascular foramina are distributed over the lateral surface of the maxilla, which, in the Frick material, are not always preserved. Several of these foram-
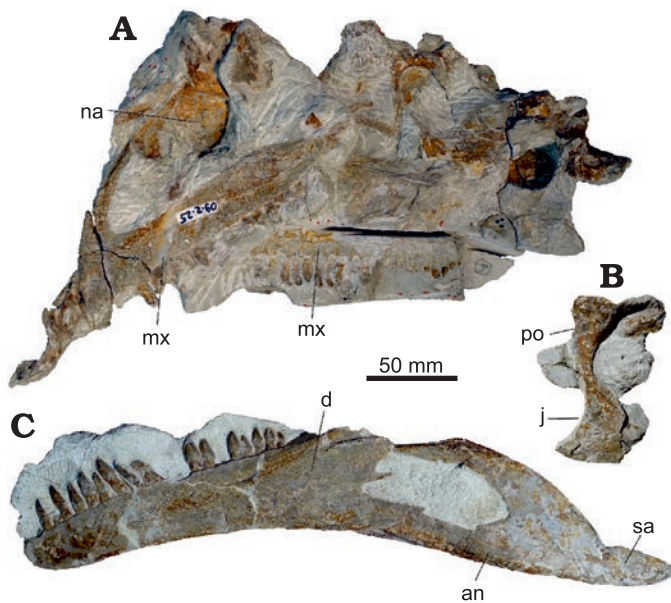
Fig. 12. Partly disarticulated skull of *Plateosaurus trossingensis* (MSF 09.2) from the Triassic of Frick, Switzerland. **A**. Main piece, showing the left lateral side of parts of the skull. **B**. Partial right postorbital and jugal in lateral view. **C**. Lower jaw in lateral view. Abbreviations: an, angular; d, dentary; j, jugal; mx, maxilla; na, nasal; po, postorbital; sa, surangular.

ina are arranged in a row, where the posteriormost foramen is the largest. In NAAG_00011238, MSF 12-4, MSF 11.4, and MSF 23, the dorsoventral diameter of the posteriormost foramen is almost one-third of the height of the lateral surface of the maxilla. This foramen is distinctively opened posteriorly, forming a groove that gradually decreases in depth posteriorly (e.g., Fig. $8A_1$). In the juvenile specimen MSF 12.3, this groove is especially pronounced and long, extending for at least 15% of the total length of the laterally exposed surface of the maxilla (Fig. $8A_1$, A_3). The more anterior foramina of the row open anteroventrally when their morphology is readily preserved; this orientation is best seen in SMNS 13200 from Trossingen. In NAAG_00011238, the row comprises at least six foramina, all located ventral to the antorbital fossa (Fig. 7A). As preserved in this skull, these foramina are comparatively small except for the penultimate and especially the ultimate one; at least three additional foramina are present on the dorsal process. In other skulls, including MSF 11.4, MSF 23, MSF 15.4, and MSF 12.3, the row comprises fewer (between two and four) but larger foramina. In SMNS 13200, the row consists of eight foramina on the left and six on the right side; this discrepancy can be either explained by single foramina not being preserved, or by asymmetry of the original foramina count. However, the preserved foramina on both sides are large, and their position and relative spacing is not compatible between the two sides, indicating at least some degree of skull asymmetry, which also suggests that foramina count differs between individuals. Outside the row, additional foramina are typically present in the recessed region of the maxilla just anterior to the base of the dorsal process, and on the anterior border of the dorsal process, as best seen in NAAG_00011238, SMNS 52968, SMNS 13200, GPIT-PV-30784, and MB.R.1936.

The dorsal process of the maxilla comprises the anterior rim, which is continuous with the lateral surface of the maxilla, and the medial sheet, which is a recessed area posterior to the rim that forms the medial wall of the antorbital fossa. At its distal end, the dorsal process articulates with the anterior process of the lacrimal; this articulation is hidden from view by the overlapping nasal. The orientation and shape of the dorsal process is highly variable, which can partly be attributed to plastic deformation. The anterior rim is oriented dorsally to posterodorsally at its base but often becomes more inclined distally. In MSF 11.4, the anterior rim is steep and its posterior margin only slightly curved, rising at 50° relative to the main body of the maxilla (Fig. $4A_1$–A_4). A distal extension is abruptly deflected posteriorly, resulting in a trapezoidal shape of the anterior half of the antorbital fossa. Similar morphologies are seen in MSF 16.1 (Fig. 3), MSF 23 (Fig. 6A), and SMA 09.1 (Fig. 10A). In the latter, the anterior rim terminates at the anterodorsal corner of the antorbital fossa, while the medial sheet continues to extend posteriorly after a sudden kink. In other skulls, the anterior rim is curved along its length to varying degrees, resulting in a more oval shape of the anterior half of the antorbital fossa, as best seen in NAAG_00011238 (Fig. 7A). As seen in some skulls from Trossingen, the posterior edge of the anterior rim can be straight while the anterior edge is strongly convex, which is most evident on the right side of SMNS 62968 but also seen in SMNS 13200. In some skulls, such as MSF 15.4, the anterior rim rises at a much lower angle (Fig. 5A). This angle as well as the curvature of the process may be exaggerated due to dorsoventral compression, and both features can vary between the left and right sides of the same skull (e.g., MB.R.1937).

The medial sheet of the dorsal process of the maxilla is highly variable in both shape and extension. In MSF 11.4 and MSF 16.1, the medial sheet occupies 50% of the antorbital fossa when measured along the greatest diameter of the latter (Figs. 3, $4A_1$–A_4). In MSF 15.4, on the other hand, the medial sheet only extends to 35% (Fig. 5A). The posterior margin of the medial sheet shows a pronounced crescent shape in the maxilla of NAAG_00011239, but is more or less straight in MSF 11.4. In NAAG_00011238, the posterior margin is straight along most of its length, but abruptly bends posteriorly in its dorsalmost section (Fig. 7A). The posterior margin of the medial sheet is concave in SMA 09.1, but the dorsal section again shows an abrupt bending. Pronounced left-right asymmetry in the shape of the medial sheet is seen in the skulls MB.R.1937 and SMNS 13200. In MB.R.1937, the medial sheet of the right maxilla is crescent-shaped while that of the left maxilla is much more straight. On the right side of SMNS 13200, the posterior edge of the medial sheet is vertical in its dorsal half but abruptly becomes much less inclined in its ventral half; these features are much less pronounced on the left side of the same skull. This asymmetry suggests that the shape of the medial sheet is of limited use for taxonomy.

Nasal: The nasal is a thin bone roofing much of the anterior and anterolateral portions of the snout. The nasal accounts for more than half the length of the skull roof in the three specimens from Frick that allow precise measurement of this character (MSF 11.4, MSF 12.3, MSF 15.4). These proportions are also found in skulls from Trossingen and Halberstadt and are a distinguishing feature of *Plateosaurus* (Galton and Upchurch 2004). The nasal has two anteroventral processes, the premaxillary and maxillary processes, which form the dorsal and posterior margins of the external naris, respectively. The premaxillary process is a thin and rod-like element that is uniform, or slightly decreasing, in dorsoventral height along its length. In dorsolateral view, it may appear broader and thinning out distally to a greater degree. Variation of this feature is therefore likely the result of different orientations of the main axis of deformation.

The maxillary process contacts the posterior process of the premaxilla ventrally, excluding the maxilla from the external naris. This feature is present in *Plateosaurus* and *Efraasia*, while in other basal sauropodomorphs the maxilla is not excluded from the external naris (Yates 2003; Galton and Upchurch 2004). In the skulls from Frick, this condition is preserved in NAAG_00011238 and in MSF 15.4. The maxillary process appears to not have reached the premaxilla in GPIT-PV-30784, but this might be the result of disarticulation. The anterior margin of the maxillary process is sinuous, with a convexity just dorsal to its mid-height, as seen in MSF 11.4, MSF 15.4, MSF 16.1, SMNS 13200, SMNS 12949, SMNS 52968, GPIT-PV-30784, and AMNH FARB 6810 (e.g., Figs. 3–5). This convexity is not evident in NAAG_00011238 and in MB.R.1937, which might be due to an incomplete preservation of the anterior margin in these skulls. The lateral surface of the maxillary process is concave anterodorsally to posteroventrally.

A rounded shelf-like extension of the nasal overhangs the dorsal margin of the antorbital fenestra, resulting in a somewhat convex profile of the latter, as seen in NAAG_00011238, MSF 15.4, GPIT-PV-30784, the right side of SMNS 13200, SMNS 12949, and MB.R.1937. This convex overhang is apparently absent in MSF 11.4 (Fig. 4A$_1$–A$_3$), but also missing on the left side of SMNS 13200, which can possibly be attributed to deformation. Just posterior to the posterodorsal corner of the external naris, the nasal is swollen, which is most pronounced in MSF 15.4 (Fig. 5A). In lateral view, this swollen part forms an apex of the dorsal margin of the nasal, while the dorsal margin posterior to this apex is concave, as best seen, among the Frick skulls, in MSF 16.1, MSF 11.4, and MSF 15.4 (Figs. 3–5). The dorsal margin of the nasal may appear convex along its length as in NAAG_00011238, which is an effect of the direction of view captured by the strongly compressed skull roof. In MSF 11.4, the concave part of the nasal posterior to the apex is sharply defined and separated from the lateral surface of the nasal by a pronounced rim (Fig. 4A$_1$, A$_3$). This depression and rim are not present or only very weakly pronounced in the other skulls, and are probably exaggerated by the strong

mediolateral compression of MSF 11.4. The suture that separates the right and left nasal is located in a longitudinal depression in all skulls where it can be observed; this region is crushed in all specimens.

In the posterodorsal corner of the nasal, the lateral surface of the nasal extends posteriorly into a hook-like process that extends onto the lateral surface of the anterior flange of the lacrimal. This process is preserved in MSF 11.4 and MSF 15.4 from Frick, MB.1927.19.1. from Halberstadt, and SMNS 13200, SMNS 12949, and GPIT-PV-30784 from Trossingen. Typically, the process is rounded and broad, especially in MSF 11.4 (Fig. 4A$_1$–A$_4$). In SMNS 12949 and GPIT-PV-30784, in contrast, it is narrow and pointed (Figs. 5B, 6B). The process is long and finger-like on the left side of SMNS 12949, but short on the right side (Fig. 5B). As best seen in MSF 11.4 and SMNS 12949, the hook-like process delimits a subrectangular embayment of the posterior margin of the nasal in dorsal view (Figs. 4A$_1$–A$_4$, 5B). This embayment receives the anterior processes of the lacrimal in SMNS 12949 and in MSF 11.4, probably also the prefrontal. Medial to this embayment, the nasal greatly extends posteriorly to contact the frontal. This posterior extension of the nasal is best seen in GPIT-PV-30784 from Trossingen, where it reaches at least 70% of the anteroposterior length of the prefrontal (Fig. 6B).

Prefrontal: The prefrontal forms the anterodorsal corner of the orbit and consists of an anterior flange, a posterior process, and a ventral process. The prefrontal is highly variable in the examined skulls. It is well preserved on the right side of MSF 11.4 (Fig. 4A$_1$–A$_4$) and on both sides of GPIT-PV-30784 (Fig. 6B). In GPIT-PV-30784, its thin anterior lamina partly overlaps the posterodorsal part of the lacrimal, leaving the anterior dorsal surface of the latter exposed in dorsal view. This overlap seems to be more extensive at least in AMNH 6810 (Prieto-Márquez and Norell 2011). The overlap is more extensive medially, as also seen in MSF 15.4, but does not reach as far anteriorly as the dorsally exposed surface of the lacrimal. MSF 11.4, in contrast, shows rectangular margin between the prefrontal and lacrimal in dorsal view, with an anterior process of the prefrontal located medial to the dorsally exposed surface of the lacrimal. This process extends anteriorly at least to a point above mid-length of the antorbital fossa, and appears to fit, together with the lacrimal, into an indentation formed by the posterior margin of the nasal.

In both sides of GPIT-PV-30784, the anterior margin of the anterior flange of the prefrontal shows a small but distinct notch (Fig. 6B), which is also seen in SMNS 13200. This notch is absent in MSF 11.4; the region is not well-preserved in other skulls. The anterior flange continues ventrally, overlapping parts of the lateral surface of the lacrimal, before terminating in a distinct step just dorsal to the lacrimal duct. This step is subrectangular in MSF 11.4, SMNS 13200, and SMNS 52968. In GPIT-PV-30784, MSF 15.8B, and MSF 15.4, in contrast, it forms a hook-like, ventrally directed tip (Figs. 5A, 6B, 9B). Ventral to the step, the ventral process of the prefrontal is twisted to articulate with the medial surface of the lacrimal, as seen in MSF 15.8B (Fig. 9D). In lateral

view, the ventral process is often covered by the lacrimal and thus hidden from view in articulated skulls, but is visible in MSF 15.4 and GPIT-PV-30784, where it leads down to more than two thirds of the anterior rim of the orbit.

The robustness of the prefrontal varies; in the skulls from Frick, it is especially massive in NAAG_00011238, while it is most gracile in MSF 11.4, in the late-stage juvenile MSF 12.3, and in the juvenile MSF 15.8B. In MSF 15.4, MSF 15.8B, and NAAG_00011238, the prefrontal is mediolaterally widest just dorsal to the ventral process, resulting in a triangular shape of the bone in dorsal view. The widest point is slightly posterior to the ventral process in MSF 16.1 and GPIT-PV-30784. In lateral view, the dorsal margin of the prefrontal forms an apex at this point. The prefrontal, and especially its posterior process, appears to be elongated in some skulls (e.g., MSF 12.3, MSF 15.8B, and especially in GPIT-PV-30784; Fig. 6B) but short and squat in others (e.g., MSF 11.4, MSF 17.4, SMNS 13200). These proportions are at least partly influenced by plastic deformation, as demonstrated by the dorsoventrally compressed MSF 12.3, where the right prefrontal is short and squat while the left is elongated (Fig. 8A$_1$, A$_2$). In this skull, the right prefrontal is slightly angled anteroposteriorly relative to the skull roof, resulting in some degree of anteroposterior shortening, while the left prefrontal is angled mediolaterally, resulting in mediolateral shortening.

The posterior process of the prefrontal is enlarged, restricting the frontal contribution to the orbit, which is considered a derived feature of *Plateosaurus* (Yates 2003). An enlarged posterior process can be observed in all skulls where the posterior process is present, including the two juvenile specimens (MSF 12.3 and MSF 15.8B; Figs. 8, 9B). In dorsal view, the posterior process is tapering distally in most skulls (e.g., MSF 12.3, SMNS 13200), but is broadly rounded in MSF 11.4 (Fig. 4A$_1$–A$_4$), GPIT-PV-30784, and MB.R.1937. However, some variation in this feature occurs between the left and right sides of SMNS 13200, and it is possible that the distal tapering is exaggerated by plastic deformation as the result of the oblique orientation of the prefrontal relative to the skull roof. In dorsal view, the lateral margin of the posterior process tends to be convex proximally and slightly concave distally. It is, instead, strongly concave on the right side of MSF 16.1 and the left side of MSF 12.3 (Fig. 8A$_1$, A$_2$). In both cases, this concavity is much less pronounced on the respective opposite side of the skull, suggesting a strong deformational influence. In MSF 11.4, the lateral margin of the prefrontal is step-like in dorsal view, narrowing the prefrontal abruptly rather than continuously as is the case in other skulls (Fig. 4A$_3$, A$_5$, A$_6$). SMNS 13200, however, shows an intermediate morphology, and at least parts of the observed variability may be the result of deformation. In MSF 16.1, MSF 15.4, and SMNS 12949, the dorsolateral margin of the prefrontal at, and posterior to, the widest point forms a bulge-like ridge that is semicircular in dorsal view and overhangs the anterodorsal portion of the orbit; this ridge is not evident in other skulls.

Lacrimal: The lacrimal separates the antorbital fenestra from the orbit, and consists of a subvertical main body and an anteriorly directed process that is overlapped by the nasal and thus hidden from lateral view in fully articulated skulls. The lacrimal is tilted anteriorly in all skulls by about 30° to the vertical; this angle is exaggerated in cases of dorsoventral deformation, as seen in NAAG_00011238 (Fig. 7A). An extensive anterior flange extends from the main body into the antorbital fenestra, resulting in the oblique posterior margin of the latter. This large flange is thought to be a derived feature of *P. trossingensis*, distinguishing it from the closely related *Efraasia* and, possibly, *P. gracilis*, which only show a narrow rim surrounding the posterodorsal corner of the antorbital fenestra (Yates 2003). The dorsoventral extent of this overhanging flange is variable as preserved in the examined skulls: the flange is less extensive and only overhangs the dorsal half of the antorbital fenestra in MSF 15.4 (Fig. 5A), while it overhangs almost the complete dorsoventral height of the antorbital fenestra in SMNS 13200 and GPIT-PV-30784. The dorsal half of the anterior margin of the anterior flange is convex, as seen in NAAG_00011238 (Fig. 7A) and MSF 11.4 (Fig. 4A$_1$–A$_4$). It appears to be concave in MSF 15.4 (Fig. 5A–C) and MSF 16.1 (Fig. 3A–D), which may be caused by deformation as this feature may vary between the left and right sides of the same skull, as is the case in MB.R.1937. Chapelle et al. (2019) note that this flange is convex in *Ngwevu* and *Lufengosaurus* but not in *Massospondylus*.

In MSF 11.4, MSF 15.4, MSF 16.1, and NAAG_00011238, the dorsolateral edge of the lacrimal forms a prominent ridge that originates ventral to the bulbous posterodorsal corner of the lacrimal and is continuous with the lateral margin of the anterior process, overhanging the anterior flange. The concavity ventral to this ridge received the posterolateral process of the nasal, as seen in MSF 15.4 (Fig. 5A) and GPIT-PV-30784 (Fig. 6B). In MSF 15.4, the ridge only originates anterior to the bulbous surface and is very narrow (Fig. 5A). In MSF 16.1, the ridge is very extensive and pronounced, and at least in this case is likely exaggerated by a medial displacement of the anterior flange due to deformation (Fig. 3). The ridge is present in SMNS 52968, but not pronounced in GPIT-PV-30784 and SMNS 13200.

The ventral end of the lacrimal is anteroposteriorly expanded. The anterior margin of this expanded part is straight and only becomes somewhat concave just dorsal to its contact with the jugal and maxilla, as seen in MSF 16.1 (Fig. 3A$_1$, A$_2$), MSF 15.4 (Fig. 5A), MSF 23 (Fig. 6A), as well as in SMNS 12949, SMNS 52968, and GPIT-PV-30784 from Trossingen and MB.R.1937 from Halberstadt. It is, however, more concave in AMNH FARB 6810 and strongly concave on the right side of SMNS 13200.

Postorbital: The postorbital is a triradiate bone forming the posterior margin of the orbit, the dorsal and anterodorsal margin of the infratemporal fenestra, and the anterolateral margin of the supratemporal fenestra. The anterior process is the shortest and stoutest, and is oriented anteromedially

and slightly dorsally. It is mediolaterally broad and dorso-ventrally narrow, while the posterior process is mediolater-ally narrow and dorsoventrally broad. The anterior process has been reported to form an angle of approximately 160° with the posterior process in AMNH FARB 6800 (Prieto-Márquez and Norell 2011). This measurement is equally high in MSF 11.4, which is mediolaterally compressed, but much lower in the dorsoventrally compressed skulls of MSF 12.3 (110°) and MSF 17.4 (115°). The high angles seen in AMNH FARB 6800 and MSF 11.4, therefore, have to be attributed to the mediolateral compression of these skulls. In MSF 09.1, the anterior process appears to be very foreshortened and triangular in lateral view (Fig. 10C). This strong fore-shortening might have resulted from an axis of deformation close to parallel to the long axis of the process. The anterior process does not reach the posterior process of the prefrontal, allowing the frontal to contribute to the dorsal margin of the orbit, as best seen in MSF 12.3 (Fig. 8). In MSF 15.4, the pos-terodorsal corner of the orbit is formed by the lateral wing of the frontal instead of the anterior process of the postorbital (Fig. 5A). A similar configuration is seen on both sides of SMNS 13200, where the anterior process of the postorbital is bounded by the frontal in dorsal view both anteriorly and posteriorly (see section "Frontal" below).

The posterior process becomes more narrow in its distal third, receiving the anterior process of the squamosal. The posterior process is very elongated and extends up to the level of the posterodorsal corner of the infratemporal fenestra, as best seen in MSF 12.3 and GPIT-PV-30784 (Figs. 6B, 8). In MSF 23, MSF 12.3, MSF 15.4, MSF 16.1, SMNS 12949, and MB.R.1937, the posterior process shows a distinct longitu-dinal groove laterally. This groove is bordered dorsally by a longitudinal ridge, which is especially pronounced anteriorly at the base of the anterior process of the postorbital. A medial process of the postorbital contacts the parietal and forms parts of the anterior margin of the supratemporal fenestra, excluding the frontal from this opening, as can be seen in the left and right postorbitals of MSF 12.3 (Fig. 8A$_1$, A$_2$) and the left one of MSF 16.1 (see section "Parietal" below).

The central body of the postorbital shows a rugosity on its anterolateral margin that overhangs the orbit in MSF 16.1 (Fig. 3A$_3$) and GPIT-PV-30784. In all specimens, the ventral process of the postorbital reaches down to the ventral mar-gin of the orbit. Its curvature is highly variable, and may be strongly (e.g., SMNS 12949) or weakly (e.g., MB.R.1937) curved; a similar variation has been noted for other basal sau-ropodomorphs such as *Massospondylus* (Yates et al. 2011).

Squamosal: The squamosal forms part of the posterodor-sal corner of the skull, and is composed of a small main body with four processes; a short posterior process, an anterolateral process, an anteromedial process, and an elongated ventral process. In lateral view, the dorsal surface of the main body and posterior process is inclined posteroventrally and forms an angle of approximately 130° with the anterolateral process, as seen in GPIT-PV-30784 and in the isolated squamosal MSF 15.8 (Fig. 9E). This angle is sharply defined in lateral view

in GPIT-PV-30784, with a triangular apex just anterior to the base of the anterior process. This apex is not pronounced in SMNS 13200 and absent in SMNS 52967; this morphology is possibly influenced by deformation. As shown by MSF 09.1, GPIT-PV-30784, and MSF 15.8.2030, the anterior pro-cess is divided into a dorsal and a ventral lobe due to a deep lateral excavation which received the squamosal process of the postorbital. This excavation terminates posteriorly level with the posterodorsal corner of the infratemporal fenestra in MSF 09.1 (Fig. 10D), GPIT-PV-30784, and SMNS 52967; the termination is slightly posterior to this corner in MSF 12.3 (Fig. 8A$_3$–A$_5$).

The ventral process is elongated, measuring 65% of the total dorsoventral height of the infratemporal fenestra. This process appears to be very gracile in AMNH FARB 6810; it is much broader anteroposteriorly in MSF 15.8B, MSF 15.4, and GPIT-PV-30784. This variation can possibly be partly explained by different orientations of the squamosal relative to the axis of deformation. The distal end of the ventral process is often deflected posteriorly (Prieto-Márquez and Norell 2011; Chapelle and Choiniere 2018) but is straight in SMNS 52967. This distal end is twisted against its antero-posteriorly expanded proximal part, exposing the groove for articulation with the quadratojugal in lateral view (e.g., MSF 11.4 and MSF 15.8B; Figs. 4A$_1$, A$_3$, 9E). In AMNH FARB 6810, the anterolateral process forms an angle of 30° with the anteromedial process in dorsal and ventral view (Prieto-Márquez and Norell 2011). This angle, however, is strongly influenced by the mediolateral deformation experienced by this skull. The original angle was at least 60°, as shown by the dorsoventrally compressed MSF 12.3 (Fig. 8A$_1$, A$_2$).

Jugal: The jugal forms the ventral margin of the orbit and is divided into an anterior process, a dorsal process, and a posterior process. The section of the anterior process ven-tral to the orbit is dorsoventrally high as seen in MSF 11.4, MSF 15.4, and MSF 16.1 among the skulls from Frick; this is a derived character of *Plateosaurus*, distinguishing the genus from the related *Efraasia* (Yates 2003). Just ventral to the mid-height of the lateral surface of the anterior process is a longitudinal ridge, as seen in MSF 11.4 (Fig. 4A$_1$, A$_3$), MSF 17.4 (Fig. 11A$_2$), and MSF 16.1 (Fig. 3A$_3$), as well as in AMNH FARB 6810, SMNS 13200, and GPIT-PV-30784 from Trossingen and MB.R.1937 from Halberstadt. The lat-eral surface ventral to this ridge is recessed. The dorsal margin of the anterior process is concave to form the ven-tral margin of the orbit, rising to an apex anteriorly at the articulation with the lacrimal to continue to describe the circular shape of the orbit. Anterior to this apex, the dorsal margin of the anterior process shows a second concavity, which receives the posterior process of the lacrimal. The apex is very pronounced in MSF 11.4 and MSF 17.4, where it is triangular in shape; the two convexities are equally pronounced (Figs. 4A$_1$–A$_4$, 12A$_2$). In other skulls the apex and convexities are much more subtle (e.g., SMNS 12949, SMNS 52968, SMNS 13200, GPIT-PV-30784) or close to absent (MSF 15.4; Fig. 5A). The apex is weakly pronounced

on the left side of MB.R.1937 but absent on the right side, indicating asymmetry or influence of deformation. The ventral margin of the jugal may show a convexity at the level of the posterior margin of the orbit, as seen in MSF 11.4, MSF 17-4, SMNS 52967, SMNS 12949, and MB.R.1937.

In MSF 11.4, in lateral view, the posterior process is distally bifurcated into a shorter, dorsally curved process and a posteriorly directed process that is more than twice the length of the former (Fig. 4A$_1$–A$_4$). The three-dimensional nature of this bifurcation is best seen in GPIT-PV-30784 and SMNS 13200 from Trossingen, which show that the bifurcated parts represent the dorsal and ventral walls of a deep excavation that opens lateroventrally in its proximal part and laterally in its distal part (Fig. 4B). This excavation receives the anteroventral process of the quadratojugal. The dorsal process of the bifurcating part of the jugal overlaps the quadratojugal laterally, while the posterior process overlaps the quadratojugal medially and ventrally. A bifurcated posterior process is also seen in SMNS 52967, while in other skulls from Frick this feature cannot be evaluated. However, at least in AMNH FARB 6810, the posterior process of the jugal is neither excavated nor bifurcated (Prieto-Márquez and Norell 2011), indicating that this feature is variable in *Plateosaurus*.

Quadratojugal: The quadratojugal delimits the posteroventral corner of the infratemporal fenestra and consists of a main body as well as two elongated processes, an anterodorsal and an anteroventral process. Among the Frick material, the quadratojugal is best preserved in MSF 11.4, where the two processes are subequal in length and slender (Fig. 4A$_1$–A$_4$). The main body of the quadratojugal is orientated posteroventrally; it is steeply inclined in NAAG_00011238 and somewhat less inclined in MSF 16.1. In MSF 11.4, the base of the anteroventral process is approximately 35% of the height of the main body of the quadratojugal; a similar value is seen in NAAG_00011238. In contrast, MSF 16.1 from Frick, MB.R.1937 from Halberstadt, and GPIT-PV-30784 and SMNS 13200 from Trossingen, the base of the anteroventral process is much higher dorsoventrally (approximately 50% of the depth of the main body; Fig. 3A$_3$, A$_4$). The anteroventral process is distinctly curved (with a concave dorsal and a convex ventral margin) in MSF 11.4 (Fig. 4A$_1$–A$_4$) and probably in NAAG_00011238, as well as in GPIT-PV-30784 and SMNS 13200 from Trossingen. In MSF 12.3 and in the left side of AMNH FARB 6810, it is straight, while it is slightly curved in MB.R.1937. At least in the former two cases, the straight morphology can be attributed to dorsoventral plastic deformation, as also indicated by the low angle formed between the anterodorsal and anteroventral processes of the quadratojugal. Based on SMNS 13200, these processes are commonly thought to form an angle of less than 45° (Galton and Upchurch 2004) or to even be subparallel to each other and form an extended posteroventral corner of the infratemporal fenestra (Pol and Powell 2007) in *Plateosaurus*. However, these processes, in most of the examined skulls, instead form a wide angle resulting in a semicircular posteroventral corner of the infratemporal fenestra, and the angle is extremely variable and reaches 70° in MB.R.1937. The very acute angles seen in SMNS 13200, AMNH FARB 6810, NAAG_00011238 and MSF 12.3 have to be attributed, at least partly, to plastic deformation.

Frontal: The frontal forms much of the skull roof between the orbits. It is mediolaterally constricted in its anterior part, where it is laterally overlapped by the prefrontal, but becomes gradually wider posteriorly. Both frontals together form a shallow medial bulge along their midline, as seen in MSF 15.4 (Fig. 5A), MSF 17.4 (Fig. 11), and MSF 16.1 (Fig. 3A, B). The lateral margin of the frontal shows an anteroposteriorly constricted indentation in dorsal view, in which fits the posterior process of the prefrontal, as best seen in MSF 12.3 (Fig. 8) and SMA 09.1. Directly posterior to this indentation, the frontal broadens mediolaterally into a wing-like flange that is mostly overlapped by the postorbital, as seen in MSF 11.4 (Fig. 4A), MSF 12.3 (Fig. 8), and NAAG_00011238 (Fig. 7A). At the base of this flange, the frontal is exposed both in dorsal and lateral view for a short section, forming the only part of the frontal contributing to the orbit. The right frontal of MSF 17.4 shows a slight ornamentation of the exposed section (Fig. 11), though no ornamentation is evident in the juvenile specimen MSF 12.3. In MSF 15.4, SMA 09.1, and SMNS 13200, parts of the lateral margin of the lateral flange are exposed in lateral view, overlapping the postorbital; this exposed part is ornamented in the latter two skulls. In SMNS 13200, this overlapping part is slender, finger-like, and highly ornamented. This ornamentation indicates that the lateral exposure of the frontal represents intraspecific variability rather than simple disarticulation.

The posterior margin of the frontal is straight, while the posterolateral corners are strongly excavated by the supratemporal fossa, so that the dorsal surface of the frontal becomes mediolaterally restricted posteriorly. The supratemporal fossa is delimited by a semi-circular, narrow ridge that forms an overhang, as best seen in MSF 16.1 and MSF 23 (Figs. 3A$_1$, A$_2$, 6A$_1$, A$_2$), but also in MSF 12.3, MSF 11.4, and MSF 17.4 (Figs. 4A$_5$, A$_6$, 8, 11). The area bordered by this ridge was interpreted as the origin of the *Musculus pseudotemporalis* (Galton 1984). Although the frontal contributes to the supratemporal fossa, it is excluded from the supratemporal fenestra by a parietal-postorbital connection, as can be unequivocally seen in MSF 12.3 (Fig. 8A$_1$–A$_3$).

Parietal: The parietal is mediolaterally constricted at its mid-section but bears large laterally directed flanges anteriorly and posteriorly. The anterior flange borders the anteromedial portion of the supratemporal fenestra and sutures with the frontal anteriorly. As best seen in MSF 12.3, the anterior flange thins out distally to a narrow strut of bone that makes contact with the medial process of the postorbital, excluding the frontal from the supratemporal fenestra (Fig. 8A$_1$–A$_3$). This is in contrast with reconstructions of SMNS 13200 from Trossingen, in which the anterior flange is indicated to be part of the frontal, lacking the anterior flange and the parietal-postorbital contact (Huene

1926; Romer 1933; Galton 1984; Galton and Upchurch 2004). Reexamination of SMNS 13200 shows that the respective suture lines cannot be traced unambiguously in the latter skull, and that both the anterior flange and the parietal-postorbital contact were likely present, as in other basal sauropodomorphs (Galton and Upchurch 2004) and probably in all *Plateosaurus* skulls examined herein.

The suture between the frontal and the parietal is somewhat elevated to bulge-like in MSF 12.3, MSF 15.4, MSF 16.1, and MSF 17.4 (Figs. 3A$_1$, A$_2$, 5A, 8). This elevated suture forms a shelf-like eminence reaching into the otherwise circular anteromedial corner of the supratemporal fossa, as seen in MSF 16.1, MSF 12.3, and MSF 11.4 (Figs. 3A$_1$, A$_2$, 4A$_5$, A$_6$, 8). In MSF 17.4, the lateral portion of the suture is developed into a rugose ridge that continues as a finger-like projection into the supratemporal fossa (Fig. 11); a similar, pronounced eminence has been listed as an autapomorphy of *Unaysaurus* (McPhee et al. 2019). Fusion of the parietals has been listed as a variable feature in *Plateosaurus* and *Massospondylus* (Galton and Upchurch 2004). The suture between the left and right parietal is unfused in all specimens from Frick; in MSF 23, the parietals are disarticulated along the suture. The suture is not clearly visible in SMNS 13200 and SMNS 12949 from Trossingen. In the skulls from Frick, a pineal foramen can be observed at least in the juvenile MSF 12.3 (Fig. 8A$_1$, A$_3$); it is also present in SMNS 12949 from Trossingen, and its presence is regarded as variable in *Plateosaurus* (Galton and Upchurch 2004).

Quadrate: The partial skull MSF 08.M preserves a disarticulated, complete right quadrate (Fig. 13A$_3$). Its overall morphology closely corresponds to the left quadrate of the Trossingen skull AMNH FARB 6810 (Prieto-Márquez and Norell 2011). Differences include the strong curvature of the quadrate shaft in medial and lateral views, leading to a posterior orientation of the quadrate head, ca. 55° relative to the ventral half of the shaft. A similar curvature is seen in MSF 15.4 and MSF 11.4. Furthermore, the posterior margin of the quadrate shaft of MSF 08.M is more sigmoidal than seen in AMNH FARB 6810. Although the ventral third of the shaft is deflected laterally to a similar degree to that seen in AMNH FARB 6810 (Prieto-Márquez and Norell 2011: fig. 18.E), the dorsal half of the shaft is straight in the latter but curved laterally in MSF 08.M. The ventral surface of the quadrate of MSF 08.M closely corresponds to that of SMNS 13200 (Galton 1984), showing a deep sulcus extending anteromedially to posterolaterally that separates well-developed condyles, with the posteromedial condyle extending more ventrally than the anterolateral condyle. This configuration is also seen in MSF 15.4 (Fig. 5A$_1$, A$_2$), but is incompatible with that described for AMNH FARB 6810 (Prieto-Márquez and Norell 2011), possibly because the ventral end of the quadrate of the latter specimen was not fully ossified (Galton 1984).

Braincase: The space between the basipterygoid processes of the basisphenoid is filled by a high interbasipterygoid septum in the basisphenoid-parasphenoid MSF 15.8.1043, SMA 09.1, MSF 08.M, and MSF 07.M (Figs. 9E,

10B, 13B, 14A). Projecting ventrally from the center of the septum is a paired median process. The high interbasipterygoid septum with a medial process is an autapomorphy of *P. trossingensis* (Yates 2003; Prieto-Márquez and Norell 2011). This feature, however, shows considerable variation. In MSF 08.M and especially in MSF 07.M, the medial ridge is protruding posteriorly in ventral view (Figs. 13C, 14A) while in MSF 15.8 and SMA 09.1 it is concave (Figs. 9E, 10B). In the latter two braincases, the ventral projections are small, while they are thick and robust in the former two braincases. In MSF 07.M and AMNH FARB 6810, these projections are only weakly separated and together form a single, knob-like process (Fig. 14A). In the basisphenoid-parasphenoid MSF 15.8.1043, on the other hand, the projections are widely separated from each other and connected via a narrow ridge (Fig. 9E). In SMA 09.1, the median process is weakly pronounced due to the strong dorsoventral deformation.

The parasphenoid is located below the level of the ventral edge of the basioccipital condyle in MSF 08.M and in MSF 07.M (Figs. 13B, 14A). This character cannot be evaluated in the isolated basisphenoid-parasphenoid MSF 15.8.1043 as the basioccipital is missing; it is weakly expressed in SMA 09.1, which can probably be attributed to the strong dorsoventral deformation of its braincase. As noted by Prieto-Márquez and Norell (2011) for AMNH FARB 6810, the basal tubera are mostly formed by the basisphenoid, while their posterior ends are part of the basioccipital, as indicated by a crenulated suture line on the ventral surface of the tubera. In MSF 08.M, the suture at least partly follows the edge between the ventral and the vertical posterior surface of the basisphenoid tubera. The basisphenoid-parasphenoid MSF 15.8.1043 exposes the sutural surface with the basioccipital (Fig. 9E). The four projections of the basal tubera are especially well defined in MSF 07.M, in which the medial groove separating the interior two of these projections is very large (Fig. 14A$_2$, A$_6$). The posterior margin of the basal tubera is W-shaped, especially in MSF 15.8.

The basioccipital comprises much of the cup-shaped occipital condyle as well as the posterior parts of the basal tubera. The basal tubera are separated by a median fossa on the caudoventral side of the basioccipital. The two separate fossae in GPIT 18318a that may diagnose *P. gracilis* are absent in all five braincases from Frick. The occipital condyle is projecting posteriorly and slightly ventrally; its posterior face is somewhat swollen relative to its neck. Its posteroventral margin is expanded ventrally; this expansion is especially pronounced in MB.R.1937 from Halberstadt and AMNH FARB 6810 from Trossingen. It is less pronounced in MSF 07.M and MSF 08.M (Figs. 13C, 14A), possibly due to dorsoventral compression. The exoccipitals can be clearly differentiated from the basioccipital in MSF 07.M, where they have convex and subtriangular posterior surfaces. In the other braincases, the suture between exoccipitals and basioccipital is indistinct.

The lateral surface of the anterodorsal part of the basisphenoid, the attachment side for the *Musculus protractor*
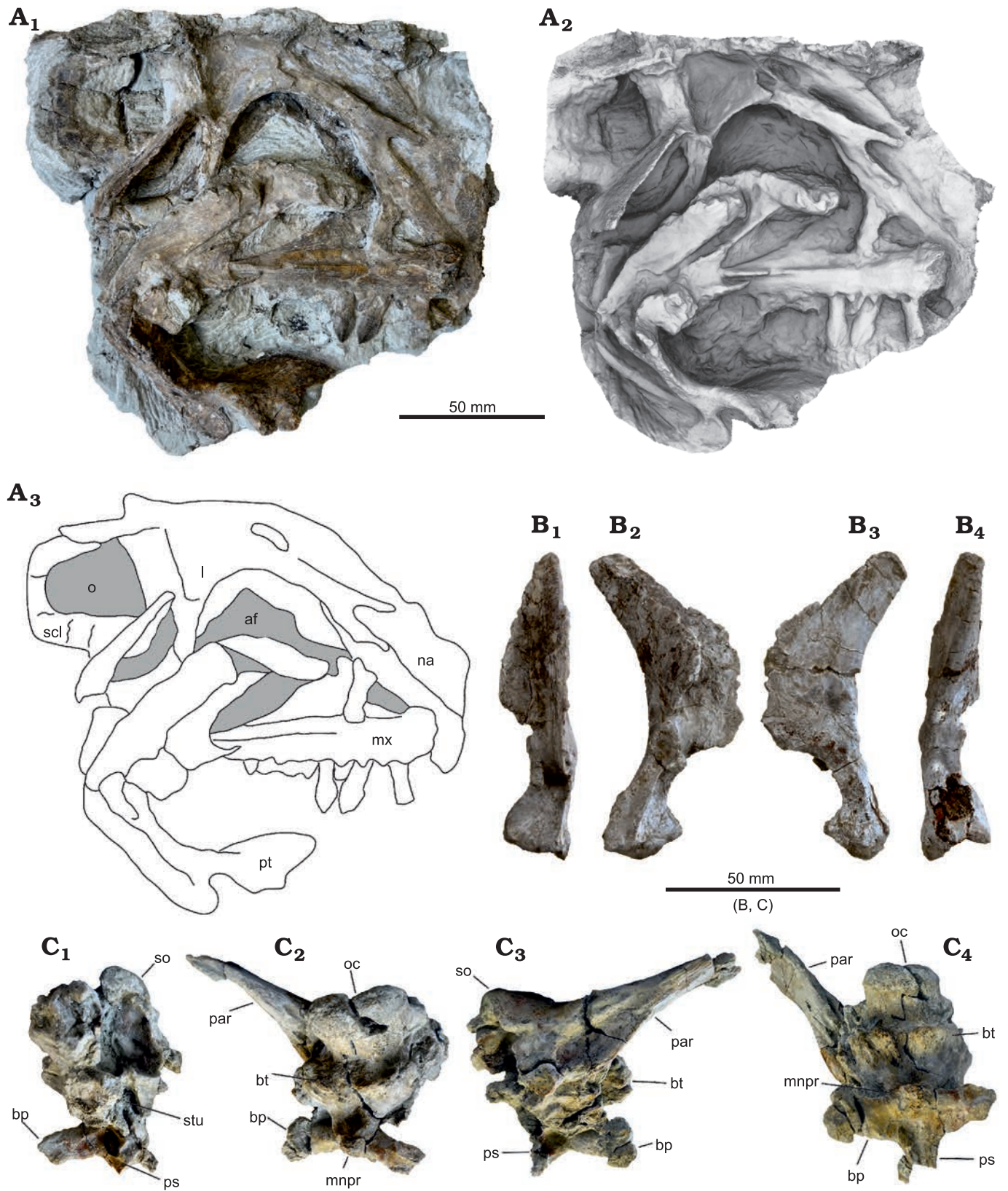
Fig. 13. **A**. Skull of *Plateosaurus trossingensis* (MSF 08.M) from the Triassic of Frick, Switzerland. **A**. Photograph of main block, skull exposed in medial view (A$_1$); ambient occlusion of photogrammetric model of the main block (A$_2$) and interpretational diagram (A$_3$). **B**. Disarticulated right quadrate in anterior (B$_1$), lateral (B$_2$), medial (B$_3$), and posterior (B$_4$) views. **C**. Disarticulated braincase in anterolateral (C$_1$), posterior (C$_2$), left lateral (C$_3$), and ventral (C$_4$) views. Abbreviations: af, antorbital fenestra; bp, basipterygoid process; bt, basipterygoid tubera; l, lacrimal; mnpr, median process; mx, maxilla; na, nasal; o, orbit; oc, occipital condyle; par, paroccipital process; ps, parasphenoid; pt, pterygoid; scl, sclerotic ring; so, supraoccipital; stu, sella turcica.
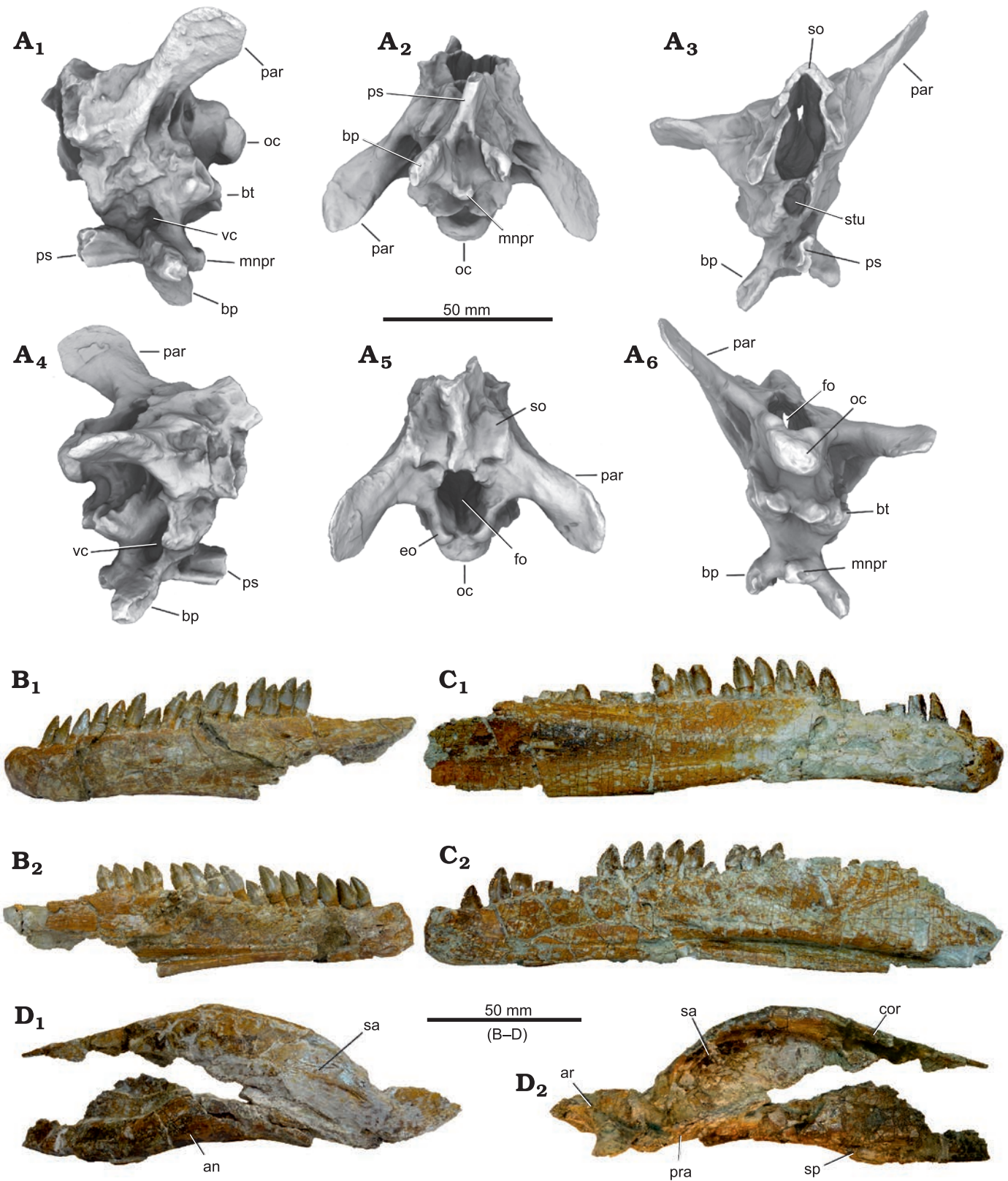
Fig. 14. Disarticulated skull elements of *Plateosaurus trossingensis* (MSF 07.M) from the Triassic of Frick, Switzerland. **A**. Ambient occlusions of photogrammetric model of the braincase in left lateral (A_1), ventral (A_2), anterior (A_3), right lateral (A_4), dorsal (A_5), and posterior (A_6) views. **B**. Left dentary in lateral (B_1) and medial (B_2) views. **C**. Right dentary in lateral (C_1) and medial (C_2) views. **D**. Posterior part of mandible in lateral (D_1) and medial (D_2) views. Abbreviations: an, angular; ar, articular; bp, basipterygoid process; bt, basipterygoid tubera; cor, coronoid; eo, exoccipital; fo, foramen magnum; mnpr, median process; oc, occipital condyle; par, paroccipital process; pra, prearticular; ps, parasphenoid; sa, surangular; so, supraoccipital; sp, splenial; sq, squamosal; stu, sella turcica; vc, exit of vidian canal.

pterygoideus, is flat and laterally offset, partly overlapping the posterodorsal part of the basisphenoid in MSF 08.M, as has been described for AMNH FARB 6810 (Prieto-Márquez and Norell 2011). This feature is very pronounced on the right side of MSF 07.M (the anterodorsal face is incomplete on the left side). Here, the anterodorsal face is not flat but dorsoventrally convex, and terminates posteriorly in a cup-shaped process overhanging the vidian canal, which is extended dorsally into a large, elongated excavation (Fig. 14A$_4$). The articulation with the laterosphenoid is well-preserved in MSF 08.M, where it is developed as a massive subrectangular process extending anteriorly and laterally from the anterodorsal part of the basisphenoid.

As seen in MSF 07.M (Fig. 13C), MSF 15.8 (Fig. 9E), and MSF 2, the lateral surface of the parasphenoid features a broad longitudinal groove that is bordered dorsally and ventrally by bulges which result in an hourglass-shape of the parasphenoid in cross-section. The ventral bulge rises posterodorsally to converge with the dorsal bulge just before the junction with the basisphenoid. The dorsal bulge is laterally expanded into a broad shelf in the posterior half of the bone, leading to a convex margin of the parasphenoid in dorsal or ventral views.

The paroccipital process is spatulate with a dorsoventrally broadened distal part. This distal end of the paroccipital process is typically asymmetrical in proximomedial view, with its distalmost point formed by a triangular apex ventral to the mid-height of the process, while the dorsal margin is broadly rounded; this morphology is seen in MSF 07.M (Fig. 14A), MSF 16.1 (Fig. 3A$_1$, A$_2$), MB.R.1936 from Halberstadt, and GPIT-PV-30784 and AMNH FARB 6810 from Trossingen. The anterior end of the prootic forms a large, elongated articular surface for the laterosphenoid.

Supraoccipital: The supraoccipital is, among the skulls from Frick, exposed in the late-stage juvenile MSF 12.3 (Fig. 8A$_1$, A$_5$) and in MSF 07.M (Fig. 14A) and MSF 08.M; well-preserved examples are also present in GPIT-PV-30784, SMNS 13200, 12949, 52967, and AMNH FARB 6810 from Trossingen and MB.R.1936 from Halberstadt. The supraoccipital reaches its greatest mediolateral breath at one third of the distance from the upper margin of the foramen magnum to the anterodorsal apex. Ventrally, the supraoccipital forms the upper third of the foramen magnum. Galton and Upchurch (2004) stated that the supraoccipital is moderately inclined at an angle of 45° in *Plateosaurus*, *Coloradisaurus*, and *Lufengosaurus*, but steeply inclined (75°) in *Anchisaurus*, *Massospondylus*, *Riojasaurus*, *Efraasia*, *Thecodontosaurus*, and *Yunannosaurus*. However, the supraoccipital is almost vertical and on roughly the same plane as the opening of the foramen magnum in MSF 07.M, SMNS 12949, and MB.R.1936. It is inclined at 30° relative to the plane containing the foramen magnum in GPIT-PV-30784, and 55° in AMNH FARB 6810 (Prieto-Márquez and Norell 2011). The supraoccipital shows an almost horizontal orientation in MSF 12.3 (Fig. 8A$_1$, A$_2$) and in MSF 07.M (Fig. 14A$_6$). This variability indicates a strong

taphonomic influence, questioning the taxonomic informativeness of the inclination angle of the supraoccipital. The almost horizontal orientation in MSF 12.3 is at least partly the result of a strong dorsoventral deformation.

The supraoccipital of *Plateosaurus* has been suggested to be longer than wide, in contrast to *Efraasia*, where it is wider than long (Galton 1973; Yates 2003). However, due to the inclination of this element, it may be shortened mediolaterally in mediolaterally compressed skulls and dorsoventrally in dorsoventrally compressed skulls. In the analyzed skulls, the supraoccipital is typically about as wide as long when measured from the roof of the foramen magnum to its anterodorsal apex. It is slightly wider than long in the dorsoventrally compressed skull SMNS 12949, and only 68% as long as wide in the strongly dorsoventrally compressed skull MSF 12.3.

Medially, the supraoccipital forms a broad longitudinal bulge that increases in height anterodorsally. This ridge is very high in MB.R.1937 but low and indistinct in MSF 12.3, which is at least partly due to plastic deformation; the original height was somewhere in-between these extremes. Galton (1984) noted that the anterior end of the bulge forms a projecting process which was covered by the parietals. However, this feature appears to be exaggerated by mediolateral deformation in SMNS 13200, and in all skulls there is a significant gap between the supraoccipital and parietals, the postparietal fenestra. In MSF 12.3, the anterior margin of the supraoccipital is strongly concave, which is the effect of the strong dorsoventral plastic deformation of the obliquely inclined and longitudinally convex supraoccipital (Fig. 8A$_1$–A$_3$). In MSF 12.3, both proatlases are preserved in place, hiding much of the lateral margin of the foramen magnum from view.

Mandible: The dentary contains 23 tooth positions in NAAG_00011238, MSF 16.1, MSF 23, and MSF 1, and 22 tooth positions in the right dentary of MSF 07.M. MSF 09.2 shows at least 20 tooth positions; it is possible that the posteriormost tooth positions are not preserved in this specimen. The early-stage juvenile MSF 15.8B had fewer than 20 tooth positions (Fig. 9B). Below the alveolar margin is an irregular row of foramina, which is best seen in MSF 01 and MSF 16.1. MSF 01 preserves at least nine foramina, which are closely spaced at the anterior tip of the dentary (distance between foramina approximately one tooth position) but become subsequently more widely spaced and larger posteriorly. MSF 16.1 only preserves the larger five posterior foramina (Fig. 3). In both specimens, the posteriormost foramen extends into a long, shallow groove extending posteriorly.

A downturned dentary with a downturned tip has been proposed to constitute an autapomorphy of *Plateosaurus* (Yates 2003). This is the case in all skulls from Trossingen and Halberstadt. Skulls from Frick, however, show a stronger variability: Although the dentary as a whole is curved ventrally in all specimens except for NAAG_00011238 (where it is straight), the distal tip is markedly curved ventrally in MSF 1, MSF 23 (Fig. 6A), and MSF 11.4 (Fig. 4A$_1$–A$_4$), but is only weakly curved in MSF 09.2 (Fig. 12), MSF

16.1 (Fig. 3), and MSF 12.3 (Fig. 8). In NAAG_00011238, MSF 07.M, MSF 15.8B, and MSF 33, the anterior tip is deflected dorsally (Figs. 7A, 9D, 14B, C).

The posterior end of the dentary is twice as high as the anterior end in all cases, as has also been reported for AMNH FARB 6810 (Prieto-Márquez and Norell 2011). The dentary is bifurcated posteriorly into a dorsal and a ventral process. In MSF 09.2, the dorsal process is bifurcated into a narrow ventral strut of bone and a broader dorsal extension (Fig. 12). This region is overlapped by the surangular in articulated mandibles (e.g., MSF 16.1). The gap between the ventral and dorsal processes of the dentary is V-shaped and walled medially by the prearticular, exposing this bone in lateral view, as seen in MSF 16.1 (Fig. 3). The prearticular forms the anterior and ventral margins of the mandibular fenestra.

Dentition: The dentition is generally in accordance with the detailed descriptions for Trossingen and Halberstadt material by Galton (1984) and Prieto-Márquez and Norell (2011), and we restrict ourselves to discussing variability of these features in the Frick material. As in the Trossingen and Halberstadt material, tooth crown height drastically decreases posteriorly in the upper jaw. In the dentary, crown height increases in the first third (e.g., MSF 1) or first half (e.g., SMA 09.1) before gradually decreasing posteriorly. Prieto-Márquez and Norell (2011) noted that in AMNH FARB 6810, tooth crowns are tilted anteriorly in the maxilla but vertical in the dentary. However, in MSF 07.M, the dentary teeth are strongly tilted posteriorly, which at least in this case is most probably is the result of deformation (Fig. 14B, C). The lingual sides of the premaxillary teeth show pronounced longitudinal striations in MSF 15.8B (Fig. 9A), which has also been noted for AMNH FARB 6810 (Prieto-Márquez and Norell 2011).

Discussion

Taxonomy

The taxonomy of *Plateosaurus* from the bonebeds of Trossingen, Halberstadt, and Frick has been a matter of much debate. *Plateosaurus engelhardti*, the former type species, was named by Meyer (1837) based on a partial postcranium discovered at Heroldsberg near Nürnberg, Bavaria, Germany. A large number of species and genera have been named since (Weishampel and Chapman 1990). Galton (1984, 1985, 1986), based on cranial material, recognized *P. engelhardti* (= *P. trossingensis*) as the only sauropodomorph species present in the bonebeds of Trossingen, Halberstadt, and, possibly, Frick, synonymizing many of the previously named species. Later, however, he recognized that the syntypes of *P. engelhardti* differ in features of the sacrum and femur from the material of Trossingen and Halberstadt, for which he resurrected *P. longiceps* (Galton 2000, 2001b; Galton and Upchurch 2004), which was originally named by Jaekel (1914) for material

from Halberstadt. Galton (2001a) recognized that *P. erlenbergiensis*, named from Trossingen material in 1908 (Huene 1908), had priority over *P. longiceps*, but considered the former a nomen dubium. Yates (2003) commented that if the interpretation of Galton (Galton 2000, 2001b; Galton and Upchurch 2004) is correct, the material from Trossingen would belong to a different taxon, although the concept of *Plateosaurus* was based on the well-preserved Trossingen skeleton SMNS 13200 much more than on the incomplete holotype. For this reason, Yates treated SMNS 13200 as the unofficial holotype of *P. engelhardti*. Moser (2003) questioned the interpretation by Galton, arguing that the supposed differences to the Trossingen and Halberstadt material resulted from an erroneous anteroposterior orientation of the sacrum. Consequently, he synonymized *P. longiceps* and other proposed species including *P. erlenbergiensis* with *P. engelhardti*. Prieto-Márquez and Norell (2011) argued that *P. erlenbergiensis* has to be considered the valid species for the material from Trossingen and Halberstadt given the priority of the name over *P. longiceps*. Galton (2012, 2013) proposed to designate *P. trossingensis* as the new type species, and SMNS 13200 as the new holotype, to conserve the traditional concept of *Plateosaurus*, as was recently decided by the International Commission on Zoological Nomenclature (ICZN 2019).

Yates (2003) distinguished between two species of *Plateosaurus*: *P. engelhardti* (= *P. trossingensis*) and *P. gracilis*. Although the skull GPIT 18318a from the Untere Mühle of Trossingen, less than a kilometer from the *Plateosaurus* bonebeds at Obere Mühle, is distinct from *P. trossingensis* and probably referable to *P. gracilis* (Yates 2003), it stems from a slightly older unit, the middle Löwenstein Formation (Hungerbühler 1998). Although *P. gracilis* is apparently absent from the bonebeds of Trossingen and Halberstadt, the possibility of its presence in Frick needs to be considered. According to Yates (2003), *P. trossingensis* can be diagnosed based on three postcranial features and the following skull features: the broad lateral sheet of the lacrimal covering the caudodorsal corner of the antorbital fenestra; the short jugal with a dorsoventrally high suborbital bar; the palatine with a centrally located, ventral, peg-like process; and the high interbasipterygoid septum that fills the whole of the space between the basipterygoid processes and has a paired median process (Yates 2003). *P. gracilis*, based on the skull GPIT 18318a, differs from *P. trossingensis* in a single autapomorphy, the paired and sharp-rimmed fossae on the basioccipital immediately behind the basal tubera. Furthermore, it shows the plesiomorphic narrow lateral sheet of the lacrimal instead of the broad lateral sheet that covers the posterodorsal corner of the antorbital fenestra in *P. trossingensis*. All skulls from Frick are in accordance with the diagnosis of *P. trossingensis* proposed by Yates (2003), although the peg-like process on the palatine could not be evaluated on any of the skulls from Frick. The two differences to *P. gracilis*, the lateral sheet of the lacrimal that overhangs the antorbital fenestra and the sharp-rimmed

fossae on the basioccipital, are highly variable in the skulls from Frick, but do not show the very different condition of *P. gracilis*. Consequently, the skull material provides no evidence for the presence of *P. gracilis* in Frick.

Galton and Kermack (2010) considered *P. longiceps* (as represented by MB.R.1937 from Halberstadt) and *P. trossingensis* (SMNS 13200 from Trossingen) to be separate species based on differences in the pterygoid. According to these authors, a broad and flattened posteromedial process of the pterygoid can be seen in MB.R.1937 as well as in other basal sauropodomorphs such as *Massospondylus*, while a hook-like posteromedial process that wraps around the basipterygoid processes is present in the Trossingen skulls SMNS 13200, SMNS 12949, and GPIT-PV-30784. This hook-like process was suggested to be a possible autapomorphy of the Trossingen species (Galton and Kermack 2010). The posteromedial process is not exposed in the studied material from Frick. However, different conditions of this feature have been described for *Massospondylus*. Barrett and Yates (2005) noted the presence of a broad and flattened posteromedial process in SAM-PK-1314 that is comparable with the condition in MB.R.1937. Chapelle and Choiniere (2018), on the other hand, described a hook-like medial process that wraps around the basipterygoid processes in BP/1/5241, similar to that seen in *Plateosaurus* skulls from Trossingen. Therefore, this feature is potentially variable within species of basal sauropodomorphs and requires re-evaluation. Yates (2003), assuming temporal separation between the strata of Trossingen and Halberstadt, noted that in Halberstadt specimens, the epipophyses of cervicals 2–6 do not overhang the caudal rim of the postzygapophyses, in contrast to specimens from Trossingen. However, the stratigraphic positions of these bonebeds are still under debate (Schoch 2011).

Galton (1986) recognized *P. ingens* from Niederschönthal, Switzerland, originally *Gresslyosaurus ingens*, as separate species, which was followed by subsequent studies (Yates 2007, 2010; Galton and Kermack 2010; e.g., Apaldetti et al. 2011). Both Moser (2003) and Rauhut et al. (2020), in contrast, stated that this material is generically distinct from *Plateosaurus*.

Variability in the skull of *Plateosaurus trossingensis*

Differences between localities and stratigraphy.—It is possible that groupings may become evident when separating specimens according to their stratigraphic horizon or locality. Osteological differences between *Plateosaurus trossingensis* specimens from Trossingen and Halberstadt have been reported (Yates 2003; see discussion above; Galton and Kermack 2010), but whether these differences warrant the recognition of separate species is unclear. The skulls from Frick, Halberstadt, and Trossingen show no obvious difference in size and character variability. Furthermore, there are no character states that are limited to one of these localities and occur in more than one skull.

In Frick, the stratigraphic approach is problematic because clear horizons are largely missing due to pedogenesis, and the precise age and length of the depositional time intervals are unknown. Although the Frick skulls described herein might be attributed to two separate horizons, a lower and a middle layer, it remains unknown if these horizons were separated by a significant time interval or if they have to be regarded as roughly contemporary. While most skulls stem from the lower layer, only three skulls (NAAG_00011238, MSF 11.4, and MSF 15.8B) stem from the middle layer, limiting comparisons further. No groupings based on the stratigraphy are apparent in Frick.

Ontogenetic variation and left-right asymmetries.—Due to their developmental plasticity, age is poorly correlated with size in *Plateosaurus* individuals (Sander and Klein 2005; Klein and Sander 2007), complicating the recognition of potential ontogenetic features. However, the postcranial skeleton of the early-stage juvenile MSF 15.8B is surprisingly consistent with that of adult individuals (Nau et al. 2020), possibly indicating that ontogenetic differences are not a major factor in the observed variation in skull anatomy. The preserved skull bones of MSF 15.8B also largely resemble those of adult individuals, and the only obvious ontogenetic differences are the reduced tooth count in the dentary (<20 tooth positions), the unossified tip of the premaxilla, and the reduced gap between the first premaxillary tooth and the tip of the premaxilla. Both MSF 15.8B and MSF 12.3 have 5 teeth in the premaxilla, which is the most frequent count seen in adult specimens, and MSF 12.3 has a minimum of 22 teeth in the maxilla, which again is within the range of adult specimens. The very steep dorsal process of the premaxilla of MSF 15.8B is possibly also related to ontogeny, although simple intraspecific variation or exaggeration by deformation are equally likely.

Some variable features, including the count and spacing of maxillary foramina and the shape of the medial sheet of the maxilla, in some cases cannot be attributed to preservation but differ between the left and right sides of a single skull. Such asymmetries indicate intraspecific variability without taxonomic relevance.

Intraspecific variability

The analyzed *Plateosaurus* cranial material is highly variable even when obvious taphonomic and ontogenetic variation is disregarded. This high degree of variation poses the question if all of it can be attributed to intraspecific variability, or if separate species might be involved. To address this question, the variable characters identified above will be divided into three groups: I, discrete characters where the dissenting character state is only found in a single specimen; II, discrete characters with dissenting character states found in more than one specimen; III, continuous characters with multiple intermediate character states.

Category I characters include: (1) the robustness of the prefrontal and postorbital, which is very pronounced in

NAAG_00011238; (2) the degree of overlap of the lacrimal by the prefrontal in dorsal view, which is much reduced in MSF 11.4; (3) the morphology of the ridge on the dorsolateral margin of the anterior process of the lacrimal, which is pronounced but narrow in MSF 15.4; (4) the posterior process of the jugal is usually bifurcated, a condition which is absent in AMNH FARB 6810; (5) the proportions of the infratemporal fenestra, which is very narrow in NAAG_00011238; (6) the dentary being straight instead of being curved ventrally, as seen in NAAG_00011238.

All skulls except for NAAG_00011238 only show a single one of these discrete unique character states, respectively. A single character may only be considered sufficient for diagnosing a separate species when it is so fundamentally different that it cannot be explained by intraspecific variability, as is the case in *P. gracilis*; even in this case, the potential species would have to be considered as preliminary (Yates 2003). Although NAAG_00011238 is distinct in three category I characters, it cannot be excluded that these features are exaggerated by deformation, and together these features are not distinct enough to warrant the recognition of a separate species. It is likely that many of the category I characters appear to be discrete only because of insufficient sample size, and instead are continuous.

Category II characters, with (a) marking the most common character state, (b) the dissenting character state, and (c) an intermediate character state: (1) the number of premaxillary teeth: 5(a) or 6(b); (2) the external naris around 0.95–1 times the length of the orbit (a) or only about 0.65 (b); (3) the ventral margin of premaxilla straight or slightly curved (a) or strongly curved (b); (4) the posterolateral process of the nasal being rounded and broad (a) or narrow and pointed (b); (5) the distal end of the posterior process of the prefrontal tapering (a) or broadly rounded (b); (6) the triangular apex of the dorsal margin of the anterior process of the jugal weakly expressed or absent (a) or pronounced (b); (7) the dorsoventral height of the base of the anteroventral process of the quadratojugal is 50% of that of the main body of the quadratojugal (a) or only 35% (b); (8) the lateral flange of the frontal is completely overlapped by the postorbital in lateral view (a) or partly exposed (b); (9) the distal end of dentary is deflected ventrally (a) or dorsally (b).

Six of these characters are dissenting in MSF 11.4, setting this skull apart from all other skulls, especially the *P. trossingensis* holotype skull SMNS 13200. However, these characters do not show any correlations with each other in the remaining skulls, with no groupings apparent (Fig. 15), and therefore are best explained by intraspecific variation.

Other character states belong to category III, continuously varying characters including intermediate states. These include: (1) the inflection at the base of the dorsal process of the premaxilla being absent (a) or present (b); (2) the anterior extent of the external naris being level with the posterior margin of the main body of the premaxilla or slightly exceeding that level (a), or extending as far as 30%

of the length of the latter (b); (3) the extent of the narial fossa reaching ca. 20% of the length of the main body of the premaxilla (a) or 30–40% (b); (4) the relative size of the antorbital fossa being typically 1.2–1.3 times the size of the orbit (a) or merely 1.1 (b); (5) the dorsoventral height of the main body of the maxilla ventral to the antorbital fossa being deep with a length-to-height ratio <4 (a) or shallow with a length-to-height ratio >4.5 (b); (6) the floor of the antorbital fossa in lateral view being concave (a) or straight to convex (b); (7) the bulge-like ridge of the prefrontal overhanging the anterior margin of the orbit being absent (a) or present (b).

The continuous nature of category III characters suggests intraspecific variability, or at least makes it difficult to define groupings (and possible species) based on them. This is despite the fact that the end-members of a continuum can be drastically different, as is the case for, e.g., the dorsoventral height of the main body of the maxilla and the size of the narial fossa. It is still possible that an extreme of a continuum is characteristic for a separate species. However, no correlations between those extremes and other character stages are evident in the examined skulls (Fig. 15). Each skull, therefore, shows a unique combination of character states without an apparent pattern.

Character/ Specimen number	MSF 23	NAA 95.1	SMA 09-1	MSF 09-2	MSF 11-4	MSF 12-3	MSF 15-4	MSF 15-8	MSF 16-1	MSF 17-4	AMNH 6010	GPIT-PV-30784	SMNS 12949	SMNS 13200	SMNS 52967	SMNS 52968	SMNS 12950	MB.R.1937
CII-1	b	a	a	–	b	a	–	a	b	–	a	a	–	b	–	a	–	b
CII-2	–	a	–	–	b	c	a	–	a	–	b	–	–	a	–	–	–	a
CII-3	a	a	a	–	b	a	a	b	a	–	a	a	a	a	–	a	a	a
CII-4	–	–	–	–	a	–	b	–	–	–	–	–	b	b	a	–	–	a
CII-5	–	–	–	–	b	a	a	a	–	b	a	b	a	a	–	?	–	b
CII-6	–	a	–	–	b	–	a	–	b	b	a	a	a	a	–	–	–	a
CII-7	–	b	–	–	b	a	–	–	a	–	b	a	a	a	–	–	–	a
CII-8	–	a	b	–	a	a	b	–	a	–	a	–	b	b	–	–	–	?
CII-9	a	b	a	a	a	a	a	b	a	–	a	a	a	a	–	a	–	a
CIII-1	a	b	a	–	a	a	–	a	–	–	a	a	–	a	–	b	a	b
CIII-2	b	c	c	–	c	a	c	c	c	–	a	c	–	b	–	b	b	a
CIII-3	–	a	a	–	b	–	–	–	–	–	a	–	–	b	–	a	a	b
CIII-4	–	a	–	–	b	–	a	–	a	–	b	–	b	a	–	–	–	a
CIII-5	a	b	b	a	c	a	a	–	a	b	b	b	–	b	a	a	b	a
CIII-6	b	a	b	b	a	a	b	–	a	a	a	b	a	a	a	c	b	a
CIII-7	a	a	–	–	a	–	b	a	b	–	a	a	b	a	–	–	–	a

Fig. 15. Overview over the distribution of variable features occurring in two or more skulls (category II and III characters; CII and CIII, respectively) in the 18 most complete skulls of *Plateosaurus* examined herein. The prevalent character state is marked with "a", while the rarer state is marked with "b". Intermediate states are marked with "c". No correlations of feature combinations that might indicate distinct species are evident, and the observed pattern is consistent with intraspecific variability.

Conclusions

Cranial material of *Plateosaurus* from Frick, Switzerland, including eight complete and six partial skulls, is described in detail for the first time. The influence of plastic deformation on aspect ratios, angular measurements, curvatures and relief are described, and an attempt is made to distinguish between osteological and taphonomic variability. We argue that the length-to-width ratio of the skull is overestimated in published skull reconstructions. Several character states of *Plateosaurus* that are generally believed to be of taxonomic importance, including the posterior extent of the tooth row and the orientation of the supraoccipital, can be explained by plastic deformation.

The described cranial material includes the first two juvenile skulls of *Plateosaurus*, belonging to an early-stage and a late-stage juvenile, respectively. The early-stage juvenile shows a reduced tooth count; an unossified tip of the premaxilla; and a reduced gap between the first premaxillary tooth and the tip of the premaxilla. The late-stage juvenile shows a proportionally large orbit. Apart from these probable ontogenetic features, juvenile anatomy is surprisingly consistent with that of adult individuals, suggesting that ontogeny might not have been a major contributing factor to the observed overall variability of the studied material.

Examination of the skull material from the bonebeds of Frick, Trossingen, and Halberstadt revealed substantial morphological variability. While parts of this variability may be attributed to taphonomic plastic deformation, a strong degree of intra- or interspecific variability is apparent, which may potentially indicate the presence of multiple species. No significant size differences between the skulls from the three localities could be detected, and most variable characters are equally variable in the different localities. To detect any possible groupings of specimens that may indicate the presence of separate species, features are categorized into discrete character states only found in one skull (6 characters), discrete character states found in more than one specimen (9 characters), and continuous characters (7 characters). Although overall variability is high, we demonstrate that each skull tends to show a novel combination of characters, and we were unable to separate the material into groups that are defined by more than one character. Consequently, the skull material from the three bonebeds bears no evidence for the presence of more than one species, but it is in accordance with the recognition of increased intraspecific variability in early dinosaurs (Griffin and Nesbitt 2016).

Acknowledgements

References

Apaldetti, C., Martinez, R.N., Alcober, O.A., and Pol, D. 2011. A new basal sauropodomorph (Dinosauria: Saurischia) from Quebrada del Barro Formation (Marayes-El Carrizal Basin), northwestern Argentina. *PLoS ONE* 6 (11): e26964.

Apaldetti, C., Martinez, R.N., Pol, D., and Souter, T. 2014. Redescription of the skull of *Coloradisaurus brevis* (Dinosauria, Sauropodomorpha) from the Late Triassic Los Colorados Formation of the Ischigualasto-Villa Union Basin, northwestern Argentina. *Journal of Vertebrate Paleontology* 34: 1113–1132.

Barrett, P.M. and Yates, A.M. 2005. New information on the palate and lower jaw of *Massospondylus* (Dinosauria: Sauropodomorpha). *Palaeontologia Africana* 41: 123–130.

Chapelle, K.E.J. and Choiniere, J.N. 2018. A revised cranial description of *Massospondylus carinatus* Owen (Dinosauria: Sauropodomorpha) based on computed tomographic scans and a review of cranial characters for basal Sauropodomorpha. *PeerJ* 6: e4224.

Chapelle, K.E.J., Barrett, P.M., Botha, J., and Choiniere, J.N. 2019. *Ngwevu intloko*: a new early sauropodomorph dinosaur from the Lower Jurassic Elliot Formation of South Africa and comments on cranial ontogeny in *Massospondylus carinatus*. *PeerJ* 7: e7240.

Etzold, A., Franz, M., and Heunisch, C. 2010. Die Forschungsbohrung Trossingen (Baden-Württemberg) und Ausführungen zum Knollenmergel und Oberkeuper der Umgebung. *LGRB-Informationen* 25: 105–142.

Fraas, P.D.E. 1913. Die neuesten Dinosaurierfunde in der schwäbischen Trias. *Naturwissenschaften* 1 (45): 1097–1100.

Galton, P.M. 1973. On the anatomy and relationships of *Efraasia diagnostica* (Huene) n. gen., a prosauropod dinosaur (Reptilia: Saurischia) from the Upper Triassic of Germany. *Paläontologische Zeitschrift* 47: 229–255.

Galton, P.M. 1984. Cranial anatomy of the prosauropod dinosaur *Plateosaurus* from the Knollenmergel (middle Keuper, Upper Triassic) of Germany. I. Two complete skulls from Trossingen/Württ. with comments on the diet. *Geologica et Palaeontologica* 18: 139–171.

Galton, P.M. 1985. Cranial anatomy of the prosauropod dinosaur *Plateosaurus* from the Knollenmergel (middle Keuper, Upper Triassic) of Germany. II. All the cranial material and details of soft-part anatomy. *Geologica et Palaeontologica* 19: 119–159.

Galton, P.M. 1986. Prosauropod dinosaur *Plateosaurus* (= *Gresslyosaurus*) (Saurischia: Sauropodomorpha) from the Upper Triassic of Switzerland. *Geologica et Palaeontologica* 20: 167–183.

Galton, P.M. 2000. The prosauropod dinosaur *Plateosaurus* Meyer, 1837 (Saurischia: Sauropodomorpha). I. The syntypes of *P. engelhardti* Meyer, 1837 (Upper Triassic, Germany), with notes on other European prosauropods with "distally straight" femora. *Neues Jahrbuch für Geologie und Paläontologie Abhandlungen* 216: 233–275.

Galton, P.M. 2001a. Prosauropod dinosaurs from the Upper Triassic of Germany. *In*: *Actas de las I Jornadas Internacionales sobre Paleontología de Dinosaurios y su Entorno: Salas de los Infantes (Burgos,*

España), septiembre de 1999, 25–92. Colectivo Arqueológico-Paleontológico de Salas, Burgos.

Galton, P.M. 2001b. The prosauropod dinosaur *Plateosaurus* Meyer, 1837 (Saurischia: Sauropodomorpha; Upper Triassic). II. Notes on the referred species. *Revue de Paléobiologie* 20: 435–502.

Galton, P.M. 2012. Case 3560 *Plateosaurus engelhardti* Meyer, 1837 (Dinosauria, Sauropodomorpha): proposed replacement of unidentifiable name-bearing type by a neotype. *The Bulletin of Zoological Nomenclature* 69: 203–212.

Galton, P.M. 2013. Comment on *Plateosaurus* Meyer, 1837 (Dinosauria, Sauropodomorpha): proposed replacement of unidentifiable name-bearing type by a neotype (Case 3560; see BZN 69: 203–212, 295–296; 70: 120–121). *Bulletin of Zoological Nomenclature* 70: 205–206.

Galton, P.M. and Kermack, D. 2010. The anatomy of *Pantydraco caducus*, a very basal sauropodomorph dinosaur from the Rhaetian (Upper Triassic) of South Wales, UK. *Revue de Paléobiologie* 29: 341–404.

Griffin, C.T. and Nesbitt, S.J. 2016. Anomalously high variation in postnatal development is ancestral for dinosaurs but lost in birds. *Proceedings of the National Academy of Sciences* 113: 14757–14762.

Galton, P.M. and Upchurch, P. 2004. Prosauropoda. *In*: D.B. Weishampel, P. Dodson, and H. Osmólska (eds.), *The Dinosauria*, 232–258. University of California Press, Berkeley.

Harris, T.M. 1974. *Williamsoniella lignieri*: its pollen and the compression of spherical pollen grains. *Palaeontology* 17: 125–148.

Huene, F. von 1908. *Die Dinosaurier der europäischen Triasformation mit Berücksichtigung der aussereuropäischen Vorkommnisse. In*: E. Koken (ed.). *Geologische und Palaeontologische Abhandlungen. Vol. 1*, 1–419. Verlag von Gustav Fischer, Jena.

Huene, F. von 1926. Vollständige Osteologie eines Plateosauriden aus dem schwäbischen Keuper. *Geologische und Paläontologische Abhandlungen, Neue Folge* 15: 139–179.

Hugi, J. and Scheyer, T.M. 2012. Ossification sequences and associated ontogenetic changes in the bone histology of pachypleurosaurids from Monte San Giorgio (Switzerland/Italy). *Journal of Vertebrate Paleontology* 32: 315–327.

Hungerbühler, A. 1998. Taphonomy of the prosauropod dinosaur *Sellosaurus*, and its implications for carnivore faunas and feeding habits in the Late Triassic. *Palaeogeography, Palaeoclimatology, Palaeoecology* 143: 1–29.

ICZN 2019. Opinion 2435 (Case 3560) *Plateosaurus* Meyer, 1837 (Dinosauria, Sauropodomorpha): new type species designated. *The Bulletin of Zoological Nomenclature* 76: 144–145.

Jaekel, O. 1914. Über die Wirbeltierfunde in der oberen Trias von Halberstadt. *Palaeontologische Zeitschrift* 1: 155–215.

Jordan, P., Pietsch, J.S., Bläsi, H., Furrer, H., Kündig, N., Looser, N., Wetzel, A., and Deplazes, G. 2016. The Middle to Late Triassic Bänkerjoch and Klettgau formations of northern Switzerland. *Swiss Journal of Geosciences* 109: 257–284.

Klein, N. and Sander, P.M. 2007. Bone histology and growth of the prosauropod dinosaur *Plateosaurus engelhardti* von Meyer, 1837 from the Norian bonebeds of Trossingen (Germany) and Frick (Switzerland). *Special Papers in Palaeontology* 77: 169.

Lallensack, J.N., Buchwitz, M., and Romilio, A. 2020. Photogrammetry in ichnology: 3D model generation, visualisation, and data extraction. *Earth ArXiv* [published online, https://doi.org/10.31223/X5J30D]

McPhee, B.W., Bittencourt, J.S., Langer, M.C., Apaldetti, C., and Da Rosa, Á.A. 2019. Reassessment of *Unaysaurus tolentinoi* (Dinosauria: Sauropodomorpha) from the Late Triassic (early Norian) of Brazil, with a consideration of the evidence for monophyly within non-sauropodan sauropodomorphs. *Journal of Systematic Palaeontology* 18: 1–35.

Meyer, H. von 1837. Mittheilungen, an Professor Bronn gerichtet. *Neues Jahrbuch für Mineralogie, Geognosie, Geologie und Petrefakten-Kunde* 1837: 314–317.

Moser, M. 2003. *Plateosaurus engelhardti* Meyer, 1837 (Dinosauria: Sauropodomorpha) aus dem Feuerletten (Mittelkeuper; Obertrias) von Bayern. *Zitteliana Reihe B* 24: 3–186.

Nau, D., Lallensack, J.N., Bachmann, U., and Sander, P.M. 2020. Postcranial osteology of the first early-stage juvenile skeleton of *Plateosaurus trossingensis* from the Norian of Frick, Switzerland. *Acta Palaeontologica Polonica* 65: 679–708.

Pol, D. and Powell, J.E. 2007. Skull anatomy of *Mussaurus patagonicus* (Dinosauria: Sauropodomorpha) from the Late Triassic of Patagonia. *Historical Biology* 19: 125–144.

Prieto-Márquez, A. and Norell, M.A. 2011. Redescription of a nearly complete skull of *Plateosaurus* (Dinosauria: Sauropodomorpha) from the Late Triassic of Trossingen (Germany). *American Museum Novitates* 3727: 1–58.

Rauhut, O.W., Holwerda, F.M., and Furrer, H. 2020. A derived sauropodiform dinosaur and other sauropodomorph material from the Late Triassic of Canton Schaffhausen, Switzerland. *Swiss Journal of Geosciences* 113: 1–54.

Reisz, R.R., Scott, D., Sues, H.-D., Evans, D.C., and Raath, M.A. 2005. Embryos of an Early Jurassic prosauropod dinosaur and their evolutionary significance. *Science* 309: 761–764.

Rex, G.M. and Chaloner, W.G. 1983. The experimental formation of plant compression fossils. *Palaeontology* 26: 231–252.

Romer, A.S. 1933. *Vertebrate Paleontology*. 491 pp. University of Chicago Press, Chicago.

Sander, P.M. 1992. The norian *Plateosaurus* bonebeds of central Europe and their taphonomy. *Palaeogeography, Palaeoclimatology, Palaeoecology* 93: 255–299.

Sander, P.M. and Klein, N. 2005. Developmental plasticity in the life history of a prosauropod dinosaur. *Science* 310: 1800–1802.

Schoch, R.R. 2011. Tracing SEEMANN'S dinosaur excavation in the Upper Triassic of Trossingen: his field notes and the present status of the material. *Palaeodiversity* 4: 245–282.

Schoch, R.R. and Seegis, D. 2014. Taphonomy, deposition and pedogenesis in the Upper Triassic dinosaur beds of Trossingen. *Palaeobiodiversity and Palaeoenvironments* 94: 571–593.

Upchurch, P. 1995. The evolutionary history of sauropod dinosaurs. *Philosophical Transactions of the Royal Society of London. Series B: Biological Sciences* 349: 365–390.

Walton, J. 1936. On the factors which influence the external form of fossil plants; with descriptions of the foliage of some species of the Palaeozoic equisetalean genus *Annularia* Sternberg. *Philosophical Transactions of the Royal Society of London. Series B, Biological Sciences* 226: 219–237.

Weishampel, D.B. and Chapman, R.E. 1990. Morphometric study of *Plateosaurus* from Trossingen (Baden-Wurttemberg, Federal Republic of Germany). *In*: K. Carpenter and P.J. Currie (eds.), *Dinosaur Systematics: Approaches and Perspectives*, 43–51. Cambridge University Press, Cambridge.

Wilson, J.A. and Sereno, P.C. 1998. Early evolution and higher-level phylogeny of sauropod dinosaurs. *Journal of Vertebrate Paleontology* 18 (Supplement 2): 1–79.

Yates, A.M. 2003. The species taxonomy of the sauropodomorph dinosaurs from the Löwenstein Formation (Norian, Late Triassic) of Germany. *Palaeontology* 46: 317–337.

Yates, A.M. 2007. The first complete skull of the Triassic dinosaur *Melanorosaurus* Haughton (Sauropodomorpha: Anchisauria). *Special Papers in Palaeontology* 77: 9–55.

Yates, A.M. 2010. A revision of the problematic sauropodomorph dinosaurs from Manchester, Connecticut and the status of *Anchisaurus* Marsh. *Palaeontology* 53: 739–752.

Yates, A.M., Bonnan, M.F., and Neveling, J. 2011. A new basal sauropodomorph dinosaur from the Early Jurassic of South Africa. *Journal of Vertebrate Paleontology* 31: 610–625.

Zahner, M. and Brinkmann, W. 2019. A Triassic averostran-line theropod from Switzerland and the early evolution of dinosaurs. *Nature Ecology & Evolution* 3: 1146–1152.